

Ru⁰ or Ru^{II}: A Study on Stabilizing the “Activated” Form of Ru-PNP Complexes with Additional Phosphine Ligands in Alcohol Dehydrogenation and Ester Hydrogenation

Daniel J. Tindall,[†] Maximilian Menche,[†] Mathias Schelwies, Rocco A. Paciello, Ansgar Schäfer, Peter Comba, Frank Rominger, A. Stephen K. Hashmi, and Thomas Schaub*

Cite This: <https://dx.doi.org/10.1021/acs.inorgchem.0c00337>

Read Online

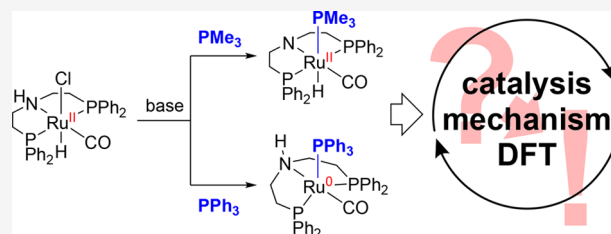
ACCESS |

Metrics & More

Article Recommendations

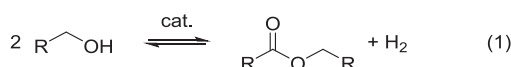
Supporting Information

ABSTRACT: The complex Ru-MACHO has been previously shown to undergo uncontrolled degradation subsequent to base-induced dehydrochlorination in the absence of a substrate. In this study, we report that stabilization of the dehydrochlorinated Ru-MACHO with phosphines furnishes complexes whose structures depend on the phosphines employed: while PMe₃ led to the expected octahedral Ru^{II} complex, PPh₃ provided access to a trigonal-bipyramidal Ru⁰ complex. Because both complexes proved to be active in base-free (de)hydrogenation reactions, thorough quantum-chemical calculations were employed to understand the reaction mechanism. The calculations show that both complexes lead to the same mechanistic scenario after phosphine dissociation and, therefore, only differ energetically in this step. According to the calculations, the typically proposed metal–ligand cooperation mechanism is not the most viable pathway. Instead, a metal–ligand-assisted pathway is preferred. Finally, experiments show that phosphine addition enhances the catalyst’s performance in comparison to the PR₃-free “activated” Ru-MACHO.



INTRODUCTION

The acceptorless dehydrogenative coupling of alcohols to esters (“dehydrogenations”) and the reverse hydrogenation of esters to alcohols with H₂ catalyzed by homogeneous transition-metal catalysts are of great interest to the chemical industry in the synthesis of bulk chemicals (eq 1).

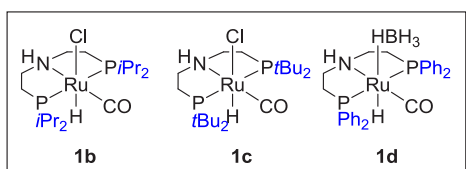
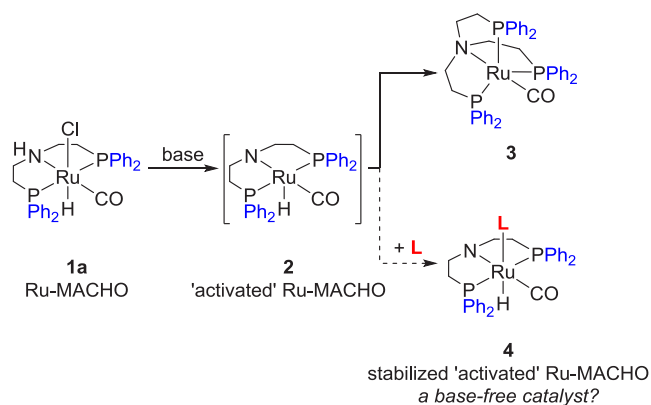


In contrast to heterogeneous processes, they can often be conducted at milder reaction conditions, reducing side-product formation.¹ Additionally, (de)hydrogenations use smaller amounts of catalysts and additives than the traditional methods with stoichiometric reagents. This, consequently, renders work-ups easier and reduces the amount of waste produced, which becomes of great importance if reactions are conducted on a larger scale. Since the pioneering work of Milstein et al.,² many important contributions have been made in this field.³ One of the systems that has been shown to be highly useful in many important transformations (e.g., hydrogenation of esters⁴ and imines,⁵ dehydrogenation of alcohols⁶ and amines,⁷ formic acid decomposition,⁸ CO₂ reduction,^{8,9} and others,^{7,10} including cross-coupling¹¹ and deuteration reactions¹²) involves the commercially available complex Ru-MACHO (1a, Scheme 1).^{4a,13} Ru-MACHO as well as its likewise commercial

derivatives 1b¹⁴ and 1c^{9a,15} requires a base (often employed in large excess) to generate the so-called “activated” 16-electron Ru^{II} complex after dehydrochlorination (i.e., in the case of Ru-MACHO, complex 2) analogous to other pincer complexes.^{4c,11a,12a,16} While the dehydrochlorinated species for 1b^{10b,j} and 1c^{6d,16b,c,e} have been isolated and structurally characterized, structural characterization of 2 still remains elusive.¹⁷ One reason for this might be the low stability of 2, as reported by our laboratory recently. In the absence of a substrate, the base-induced dehydrochlorination of 1a was followed by immediate degradation of the presumably formed 2. From the resulting plethora of ruthenium species, three could be characterized by X-ray crystallography, and their structures suggested that ligand fragmentation and reassembly must have taken place.¹⁸ Among these, the Ru⁰ complex 3, bearing a tripodal tetradentate ligand (Scheme 1), was selected for further studies and exhibited excellent catalytic activity in the (de)hydrogenations without any base necessary for activation (for hydrogenations with H₂, activation by an alcohol was required). Complex 3 represents a

Received: February 4, 2020

Scheme 1. Previously Reported Substrate-Free Formation of a Ru⁰ Complex (3) and Envisioned Route to a Base-Free Catalyst (4) through Stabilization of the “Activated” Ru-MACHO (1a)^a



^aTwo other commercially available derivatives of Ru-MACHO that require activation by a base (**1b** and **1c**) and the base-free Ru-MACHO-BH (**1d**) are depicted in the inset.

rare example of a Ru⁰ precatalyst for alcohol dehydrogenations and ester hydrogenations. Very recently, the group of Chianese showed that their Ru^{II}-CNN complexes as well as Milstein's Ru^{II}-PNN complex can undergo base-induced dehydroalkylation, yielding the corresponding catalytically active Ru⁰ complexes in the presence of PCy₃.¹⁹ While at the current stage it remains unclear if these systems involve an on-cycle Ru⁰ species, Grützmacher and co-workers have demonstrated that their system converts methanol (MeOH) and H₂O into H₂ and CO₂ via a Ru^{II}/Ru⁰ cycle.²⁰

Because of its application potential, a robust and base-free catalytic system is highly desirable.²¹ The complex Ru-MACHO-BH¹³ (**1d**, Scheme 1) shows a high activity in alcohol dehydrogenations as well as the hydrogenation of carbonyl compounds in the absence of basic additives.^{4d,f,6d,21p,r,22}

Despite this and its commercial availability, the BH₄⁻ ligand will decompose over time in these reaction mixtures by alcoholysis, resulting in a diminished long-term stability of **1d**.²³

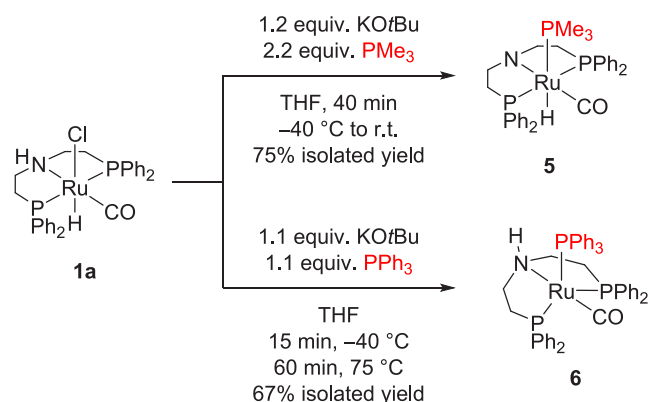
Because the previously shown degradation of **1a**, or rather **2**, is assumed to be problematic in many ways (e.g., loss of catalyst, uncontrolled formation of side products, etc.), a study was undertaken to evaluate the possibility of stabilizing the unsaturated complex **2** by a neutral L-type ligand (Scheme 1).²⁴ The hypothesized complexes of type **4** would, first, be expected to act as base-free catalysts in (de)hydrogenation reactions, which would make them applicable to a broader scope (e.g., to base-sensitive substrates) and would eliminate the challenge of dealing with the remaining amounts of base and side products thereof (e.g., salts) after the reaction is completed. Second, the ligand L is hypothesized to increase the lifetime of the catalyst in the reaction mixture and/or to aid in carrying the catalyst from one substrate batch to the next one without degradation. The only other Ru-MACHO-related system bearing an L-type ligand was reported by Ogata et al., who

substituted the CO ligand with an N-heterocyclic carbene. Although this allowed ester hydrogenations at relatively low pressures, a large excess of base was still necessary.²⁵

RESULTS AND DISCUSSION

Synthesis and Characterization of the Ru^{II} Complex 5 and Ru⁰ Complex 6. At the outset of this study, a cold solution of KO^tBu in tetrahydrofuran (THF-*d*₈) was added to a cold suspension of Ru-MACHO and PMe₃ in THF-*d*₈, resulting in an immediate color change and the dissolution of all solids after warming to room temperature and yielding a yellow solution, which was analyzed by NMR spectroscopy. The ¹H NMR spectrum showed a doublet of triplets at −8.02 ppm (*J* = 104.8 and 20.5 Hz). In the ³¹P{¹H} NMR spectrum, two signals, a doublet at 67.1 ppm (*J* = 20.7 Hz) and a triplet at −25.2 ppm (*J* = 20.7 Hz) with an integral ratio of 2:1, were detected. The data suggested that the desired complex **5** was formed selectively

Scheme 2. Synthesis of Ru^{II} Complex 5 and Ru⁰ Complex 6



(Scheme 2). Further analysis confirmed this interpretation: the ¹³C{¹H} NMR spectrum shows a signal (triplet of doublets, *J* = 11.0 and 8.8 Hz) at 206.3 ppm, which was assigned to the carbonyl carbon. The IR spectrum shows a carbonyl stretching frequency at 1885 cm⁻¹, which is in agreement with the literature data for related complexes (see, for example, ref 9a).

Crystals suitable for X-ray diffraction analysis were grown by layering a benzene solution with pentane at room temperature. The molecular structure of **5** shows a distorted octahedral geometry in which PMe₃ and the hydride ligand are oriented trans to each other, while the tridentate amido ligand coordinates in a meridional fashion (Figure 1). The fourth coordination site of the equatorial plane is occupied by the CO ligand. The distortion is most pronounced in the nonlinear coordination of the two phosphine side arms to ruthenium [P1–Ru1–P2, 158.52(2)°]. The Ru1–P3 distance [2.4007(5) Å] is significantly longer than the distances between the metal center and the phosphorus atoms of the PNP ligand [Ru1–P1, 2.3037(5) Å; Ru1–P2, 2.3109(5) Å]. Furthermore, the higher steric demand of PMe₃ compared to the hydride ligand leads to a greater distance of the two phenyl groups syn to PMe₃ [C11...C31, 7.045(2) Å] than the two phenyl groups syn to the hydride ligand [C21...C41, 6.039(3) Å]. The distance Ru1–N1 [2.157(2) Å] is only slightly shorter than that in the parent Ru-MACHO complex [2.174(2) Å⁸], indicating that the lone pair on N1 is not contributing much to stabilization of the ruthenium center because of the presence of the additional phosphine ligand [in the related complex **1b**, a much more

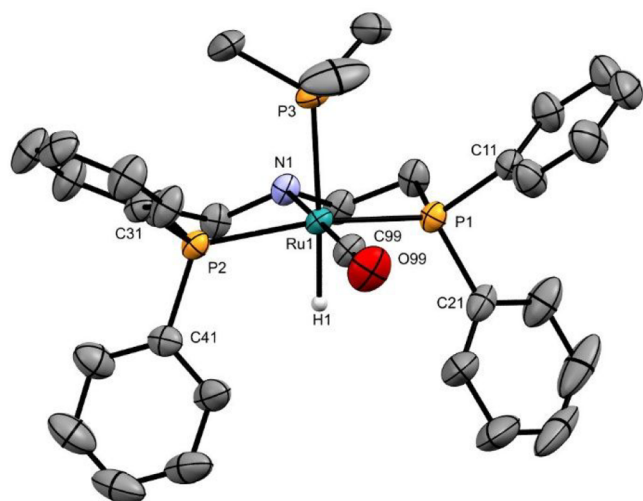


Figure 1. Molecular structure of **5** in the solid state with ellipsoids depicted at the 50% probability level. C–H hydrogen atoms and one molecule of cocrystallized benzene are omitted for clarity. Selected distances (Å) and angles (deg): Ru1–C99, 1.848(2); Ru1–N1, 2.157(2); Ru1–P1, 2.3037(5); Ru1–P2, 2.3109(5); Ru1–P3, 2.4007(5); Ru1–H1, 1.62(2); C99–Ru1–N1, 178.24(7); C99–Ru1–P1, 97.05(6); C99–Ru1–P2, 98.79(6); C99–Ru1–P3, 93.03(6); C99–Ru1–H1, 93.5(8); N1–Ru1–P3, 88.52(4); N1–Ru1–H1, 84.9(8); P1–Ru1–P2, 158.52(2); P1–Ru1–P3, 97.17(2); P2–Ru1–P3, 96.38(2); P3–Ru1–H1, 173.4(8).

pronounced contraction of the Ru–N bond is observed: 2.184(2) Å (H,H-trans isomer) versus 2.0026(8) Å^{10b} and 2.195(2) Å (H,H-syn isomer) versus 1.998(1) Å^{10j} for the parent and dehydrochlorinated complex, respectively].

When the same reaction was carried out with PPh₃ instead of PMe₃, the formation of a dark-red solution was observed. In the ¹H NMR spectrum, no signals were detected below 0 ppm, whereas the ³¹P{¹H} NMR spectrum (81 MHz) showed two signals, which appeared to be doublets of doublets at 57.7 and 52.9 ppm. Further NMR analysis proved the presence of one CO ligand ($\delta_{\text{C}} = 217.7$ ppm), whose IR frequency was determined to be 1844 cm⁻¹. Eventually, the structure was clarified by X-ray crystallography (Figure 2; **6** in Scheme 2).

The complex does not resemble a ruthenium hydride complex, and the formal oxidation state of the metal is 0. On the one hand, it contrasts with the structure of **5**, which is a ruthenium hydride complex in the formal oxidation state 2+. On the other hand, it shows a structure very similar to the previously reported complex **3**. In the solid state, the pentacoordinated Ru⁰ center adopts a distorted trigonal-bipyramidal geometry (with a structural index parameter τ of 0.81²⁶). The CO ligand occupies an axial position. The nitrogen atom of the PNP ligand—still carrying the hydrogen atom—is located trans to CO [N–Ru–C, 178.24(7)^o]. The two PPh₂ side arms coordinate to ruthenium in the equatorial position along with the PPh₃ ligand. The increased Ru–N distance [2.246(6) Å] compared to **5** [2.157(2) Å] can be rationalized by the lower oxidation state of ruthenium in **6** and matches with the Ru–N distance in the related Ru⁰ complex **3** [2.25(1) Å¹⁸]. The same reasoning allows one to understand the observed differences in the IR stretching frequencies (**3**, 1851 cm⁻¹; **5**, 1885 cm⁻¹; **6**, 1844 cm⁻¹).

The conformation of PPh₃ in **6** contrasts with the conformation of PMe₃ in **5**: one of the C–P bonds of PPh₃ is oriented anti-periplanar to the carbonyl group [torsion angle C71–P3–Ru1–C99, 165.5(4)^o], while one of the C–P bonds

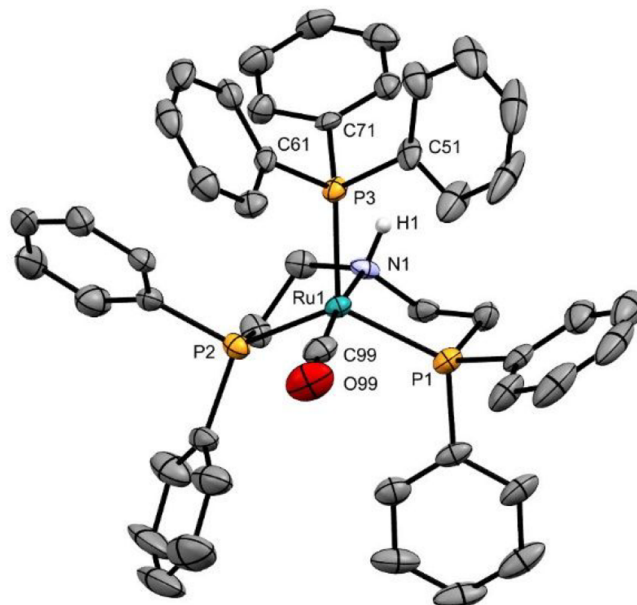


Figure 2. Molecular structure of **6** in the solid state with ellipsoids depicted at the 50% probability level. C–H hydrogen atoms and one molecule of cocrystallized benzene are omitted for clarity. Selected distances (Å) and angles (deg): Ru1–C99, 1.809(9); Ru1–N1, 2.246(6); Ru1–P1, 2.296(2); Ru1–P2, 2.307(2); Ru1–P3, 2.330(2); C99–Ru1–N1, 171.5(3); C99–Ru1–P1, 93.4(3); C99–Ru1–P2, 96.5(3); C99–Ru1–P3, 96.6(2); N1–Ru1–P3, 91.68(16); P1–Ru1–P2, 122.67(7); P1–Ru1–P3, 118.20(8); P2–Ru1–P3, 116.42(9).

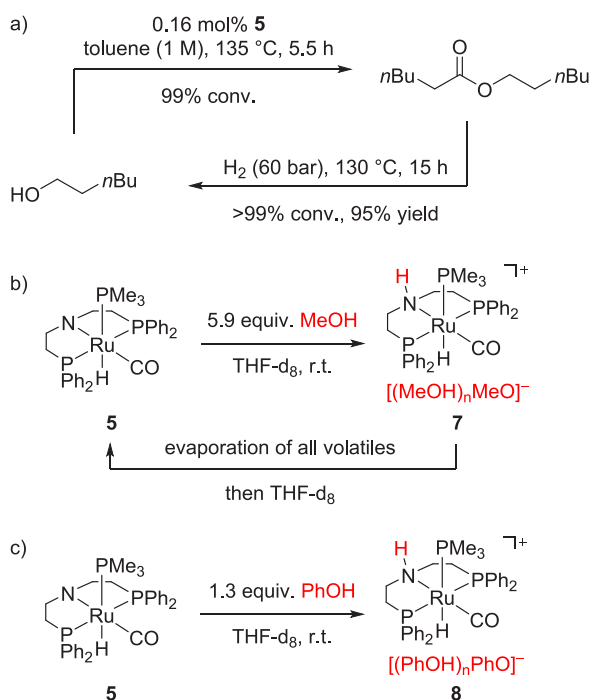
of PMe₃ adopts a syn-periplanar conformation with CO [C8–P3–Ru1–C99, 2.4(1)^o]. Intuitively, the syn-periplanar conformation should be preferred because it places two of the phosphines' substituents in a less crowded space above the two ethylene bridges of the PNP ligand rather than close to the ligands' phenyl groups. The opposite conformation in **6** places one phenyl group fairly close above the NH functionality, and the concerning Ru–P–C angle is strongly decreased compared to the other two [Ru1–P3–C71, 113.8(3)^o; Ru1–P3–C51, 120.9(3)^o; Ru1–P3–C61, 121.5(2)^o]. This structural feature was also found in the quantum-chemical calculations (vide infra). Therefore, a stabilizing N–H $\cdots\pi$ -phenyl interaction is assumed to be one of the main reasons (along with packing effects and intramolecular dispersion interactions) for the observed anti-periplanar conformation. It is concluded that this interaction as well as the greater steric demand of PPh₃ compared to PMe₃ leads to the preferred formation of the Ru⁰ complex **6** over its isomeric Ru^{II} counterpart, as is observed in the case of PMe₃.

Other phosphorus-based ligands were also tested: P(OPh)₃ was also found to trap the “activated” Ru–MACHO but was also prone to base-induced decompositions (Figure S1). The sterically highly demanding P(*t*Bu)₃ did not coordinate to the ruthenium center because a complex mixture similar to that in the reaction without any additional ligand was obtained (Figures S7–S10).

Reactions of **5 and **6** toward Alcohols and Esters.** Complexes **5** and **6** were tested as catalysts in (de)-hydrogenation reactions to evaluate whether there is any mechanistic difference of the Ru⁰ versus Ru^{II} complexes in the active species. First, **5** was used in the catalytic (0.16 mol %) dehydrogenative coupling of hexanol to hexyl hexanoate in refluxing toluene overnight. Under these unoptimized con-

ditions, a quantitative conversion [determined by gas chromatography (GC) and NMR spectroscopy] of the alcohol to the ester was observed. The reaction could be reversed (>95% GC/NMR yield) by transferring the reaction mixture under argon directly to a Premex steel autoclave, pressurizing it with 60 bar of H₂, and heating it overnight at 130 °C (Scheme 3a). Commercial hexyl hexanoate was hydrogenated under the same unoptimized conditions (>99% GC/NMR yield) but only if it was purified by distillation prior to its use.

Scheme 3. Reactivity of Complex 5 toward Alcohols and Esters: (a) Catalytic Dehydrogenation of Hexanol to Hexyl Hexanoate Followed by Hydrogenation with H₂ without Any Work-up; (b) Reversible Protonation by MeOH; (c) Protonation by PhOH



Similarly, complex 6 successfully converted hexanol into hexyl hexanoate at a comparable catalyst loading (0.15 mol %) in refluxing toluene overnight. The hydrogenation with H₂ of hexyl hexanoate (0.13 mol %) proceeded equally well under the previously mentioned conditions (>99% GC/NMR yield).

Because 5 and 6 were shown to catalyze (de)hydrogenation reactions similarly well (see Figure S35 for the corresponding kinetic data), the attention was turned to the question through which the catalytic cycles of both complexes operate. Stoichiometric NMR experiments were sought to understand the initial steps of the catalytic process.

When isolated complex 5 was reacted with the simplest alcohol, MeOH, at room temperature, an instant protonation of 5 was observed. The clean formation of complex 7 was suggested by the ³¹P{¹H} NMR spectrum (81 MHz), which showed two shifted doublets at +60.5 ppm (*J* = 18.3 Hz) and −26.6 ppm (*J* = 18.4 Hz) compared to the starting complex 5 (67.1 and −25.2 ppm). The characteristic doublet of triplets was detected in the ¹H NMR spectrum at −7.54 ppm (*J* = 86.9 and 18.9 Hz), slightly downfield from the hydride shift observed in 5 (−8.02 ppm). The overall features of the spectral data are similar to those observed for 5 with the exception that a new broad singlet was

detected at 5.36 ppm, which was assigned to the protonated amide moiety. The protonation of 5 with MeOH is reversible (Scheme 3b). Removal of all volatiles in vacuo and dissolution of the solid in THF-*d*₈ resulted in NMR spectra matching those of complex 5. The addition of MeOH resulted again in the formation of 7 (see Figure S15 for the corresponding NMR spectra).

Because no crystals of 7 could be obtained, MeOH was replaced by PhOH in the reaction with 5 (Scheme 3c). The obtained onium complex 8 showed very similar spectroscopic features in the NMR spectra compared to 7. Crystals of 8 could be grown by layering a benzene solution with pentane at room temperature, and its molecular structure was determined by X-ray diffraction analysis (Figure 3). The geometric features of the

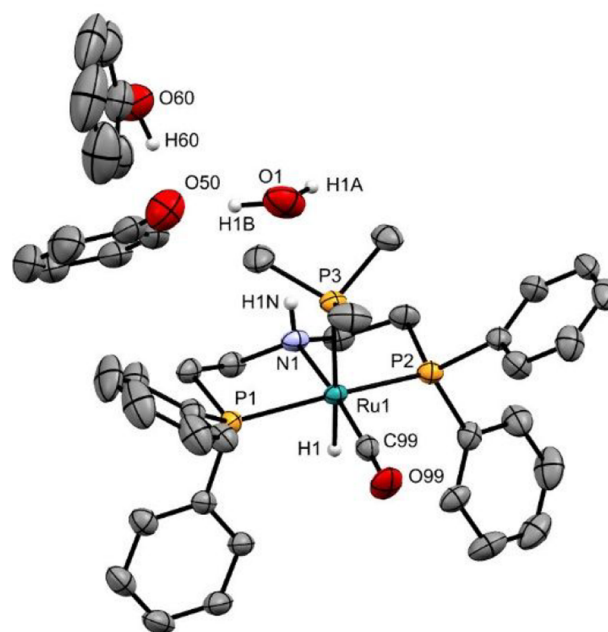


Figure 3. Molecular structure of 8 in the solid state with ellipsoids depicted at the 50% probability level. C–H hydrogen atoms and one molecule of cocrystallized benzene are omitted for clarity. Selected distances (Å) and angles (deg): Ru1–C99, 1.833(3); Ru1–N1, 2.194(2); Ru1–P1, 2.3152(8); Ru1–P2, 2.3233(8); Ru1–P3, 2.4170(7); Ru1–H1, 1.55(2); C99–Ru1–N1, 173.2(1); C99–Ru1–P1, 95.06(9); C99–Ru1–P2, 97.76(9); C99–Ru1–P3, 95.17(9); C99–Ru1–H1, 89.9(9); N1–Ru1–P3, 91.46(6); N1–Ru1–H1, 83.5(9); P1–Ru1–P2, 160.59(3); P1–Ru1–P3, 95.49(3); P2–Ru1–P3, 97.80(3); P3–Ru1–H1, 175.0(9).

of 8 are similar to those of its precursor (5): for example, both exhibit an envelope conformation of the five-membered metallacycles. Although all parameters are in a similar range, a significant effect of the protonation at the ligands' nitrogen is observed [e.g., N1–Ru1–P3: 5, 88.52(4)°; 8, 91.46(6)° or Ru1–N1: 5, 2.157(2) Å; 8, 2.194(2) Å]. The phenolate counteranion of complex 8 is imbedded in a tight hydrogen-bonding network with a molecule of PhOH [O50–O60, 2.557(4) Å] and a cocrystallized water molecule [O50–O1, 2.518(4) Å].²⁷ The latter interacts with the NH functionality [N1–O1, 2.938(4) Å]. The interactions clearly resemble the ability of the NH group to attract polar groups, which is an important feature in the mechanistic regimes presented in the literature (for example, see ref 28) as well as in this work (vide infra).

Complex 7 did not serve as a competent catalyst for the dehydrogenation of hexanol in refluxing toluene, while complex 8 did. On the one hand, a complex mixture was obtained when heating a sample of 7 in an NMR tube. It is suspected that the ruthenium center is carbonylated and/or formylated, leading to inactive species similar to those reported by Prakash and co-workers on their work on basic MeOH dehydrogenation (see the Supporting Information for a computational evaluation of this process).^{5h} On the other hand, phenolate 8 does not decompose upon extended heating; therefore, the exchange with hexanol is assumed to, consequently, furnish a productive catalytic reaction.

In contrast, complex 6 and MeOH did not react at room temperature. Upon heating, several species were observed by ³¹P{¹H} NMR spectroscopy, which looked similar to what was observed for complex 7. Therefore, MeOH was replaced again by PhOH as a surrogate alcohol. Now, a reaction occurred at room temperature, although slowly overnight. In the corresponding ¹H NMR spectrum, a new triplet (*J* = 19.9 Hz) was detected at −16.58 ppm. In the ³¹P{¹H} NMR spectrum, the signals assigned to complex 6 had disappeared and two new singlets were observed at 51.9 and −5.5 ppm. These data suggested that a ruthenium hydride had formed and the PPh₃ ligand had dissociated from the metal center, maybe even being substituted by the phenolate anion. Removing PPh₃ from this reaction mixture proved difficult and, therefore, the hypothesized product (9) was synthesized independently from Ru-MACHO (1.0 equiv) through a salt metathesis with PhOK (1.0 equiv) in the presence of PhOH (1.0 equiv). The NMR data of 9 were in accordance with those obtained in the reaction of 6 and PhOH. Crystals suitable for X-ray diffraction analysis were obtained by layering a solution in THF with pentane, and the molecular structure matches the findings in solution (Figure 4).

The PNP ligand arrangement around the metal is similar to 8 and exhibits an envelope conformation of the two five-membered metallacycles. The phenolato oxygen atom and the NH group engage in a hydrogen-bonding network with a molecule of PhOH. This structural motif is known for two different alcohols and 1b: Gusev and co-workers reported it with *i*PrO[−]/*i*PrOH (10)¹⁴ and the Gauvin group with EtO[−]/EtOH (11, Chart 1).^{28c} Despite the different substituents on the phosphorus and oxygen atoms, complex 9 is structurally very similar to 10 and 11. The major difference of the CO ligand being bent out of the equatorial plane in 9 is attributed to steric effects of the aryl versus alkyl substituents [N–Ru–C: 9, 167.4(2)°; 10, 175.2(3)°; 11, 178.09(9)°]. The distances in the hydrogen-bonding network cover a similar range [N–O: 9, 2.994(5) Å; 10, 2.864(9) Å; 11, 2.932(3) Å; O–O: 9, 2.523(5) Å; 10, 2.494(7) Å; 11, 2.495(3) Å].

It is important to note that the alcohol oxidatively adds in a trans disposition to the Ru⁰ center of 6, forming a Ru^{II} complex.^{29–31} The same 0/2+ oxidation on ruthenium was observed by us with the Ru⁰ complex 3.¹⁸ When 8 and 9 are compared, complex 8 resembles a precursor to 9, in which the transformation 8 → 9 is only precluded by the tight binding of PMe₃ to the ruthenium center.

Finally, complex 9 was shown to serve as an excellent base-free catalyst in the dehydrogenation of hexanol (0.11 mol %, refluxing toluene overnight, full conversion, and quantitative yield by GC and NMR).

Complexes 5 and 6 have been shown to lead to closely related species upon reaction with alcohols. The Gauvin group has isolated a similar species (11) derived from 1b and assigned

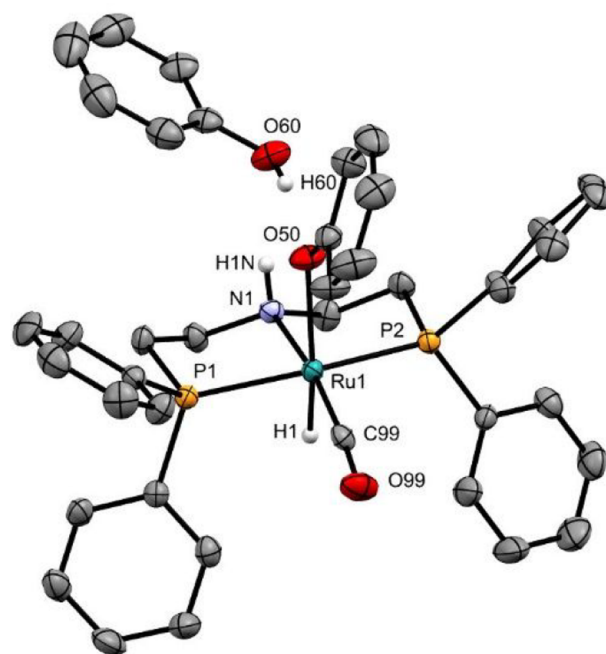
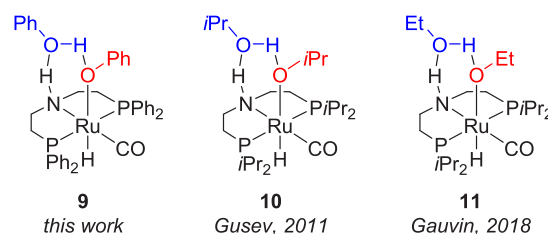


Figure 4. Molecular structure of 9 in the solid state with ellipsoids depicted at the 50% probability level. C–H hydrogen atoms and one molecule of cocrystallized THF are omitted for clarity. Selected distances (Å) and angles (deg): Ru1–C99, 1.811(4); Ru1–N1, 2.200(3); Ru1–O50, 2.234(3); Ru1–P1, 2.310(2); Ru1–P2, 2.328(2); Ru1–H1, 1.50(4); C99–Ru1–N1, 167.39(16); C99–Ru1–O50, 108.0(2); C99–Ru1–P1, 93.9(2); C99–Ru1–P2, 99.3(2); C99–Ru1–H1, 86(2); N1–Ru1–O50, 84.5(2); N1–Ru1–H1, 81(2); O50–Ru1–P1, 95.33(9); O50–Ru1–P2, 90.54(9); P1–Ru1–P2, 163.24(4); O50–Ru1–H1, 165(2).

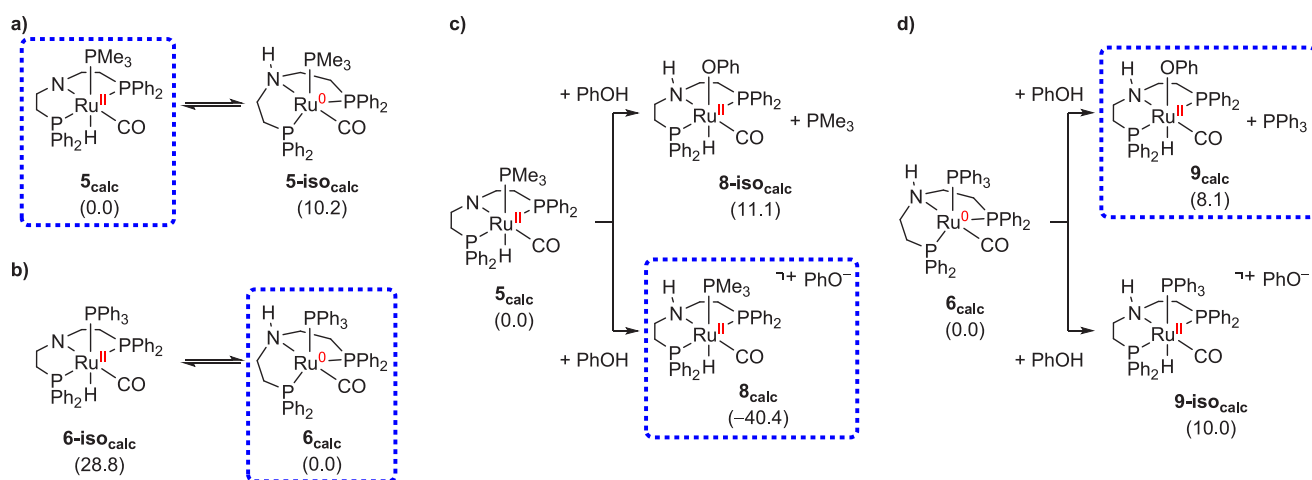
Chart 1. Ruthenium(II) Hydride Alcoholato Complexes with an Aliphatic PNP Ligand



them as a resting state of dehydrochlorinated 1b.^{28c} Because they presented detailed experimental work on the involved steps as well as on the formation of deactivation species (*vide infra*), it is assumed that 5 and 6 lead to similar catalytic cycles.

Computational Investigations. The next step was to endeavor computational methods (see the Supporting Information for details), first, to rationalize the formation of Ru^{II} complex 5 and Ru⁰ complex 6 and, second, to evaluate in which mechanistic scenarios each of the two complexes is involved. Due to the extensive interest in pincer-type catalysts for hydrogenation/dehydrogenative coupling, a variety of groups have previously performed experimental and theoretical studies on the underlying mechanisms: Beller and co-workers published a detailed investigation on complex 1b,^{10j} and Chen et al. studied Gusev's Ru–SNS complex.³² Computational investigations were also conducted for Milstein's Ru^{II}–PNN^{28a} and other related chiral pincer complexes.^{28b,33} We are only aware of two computational studies employing the full Ru–MACHO complex

Scheme 4. (a) Comparison of the Ru⁰ and Ru^{II} Stabilities for PMe₃, (b) Comparison of the Ru⁰ and Ru^{II} Stabilities for PPh₃, (c) Formation of the Phenolato Complex **8-iso_{calc}** and Onium Complex **8_{calc}** from **5_{calc}** and (d) Formation of the Phenolato Complex **9_{calc}** and Onium Complexes **9-iso_{calc}** from **6_{calc}**^a



^aExperimentally observed structures are highlighted with blue dotted lines. ΔG^{298} in kJ mol^{-1} ; RI-PBE0-D3(BJ)/def2-QZVPP//BP86/def2-SV(P); COSMO-RS (toluene).

(i.e., no simplifications in the structural complexity for the purpose of reducing computational costs).³⁴ First, Jiang et al. studied the mechanism of MeOH-to-carbonate dehydrogenation. However, MeOH is a very small substrate that has been shown to differ significantly from larger substrates in terms of interactions with the Ru-PNP fragment.^{9e,35} Second, a very recent report by Kaithal et al. on the mechanism of β -methylation of alcohols involves several steps of the Dub-type pathway (vide infra) without any detailed discussion of other mechanistic scenarios, relevant resting states, or the related literature.^{34b} In this context, we wanted to address some specific aspects that were not considered in detail so far: (1) the resting state of the catalyst, (2) the role of the $\text{HN}(\text{CH}_2\text{CH}_2\text{PPh}_2)_2$ ligand and the alcohol substrate, (3) an investigation of all possible reaction pathways, (4) the potential influence of the oxidation state (Ru⁰ versus Ru^{II}), and (5) the specific role of the NH function.

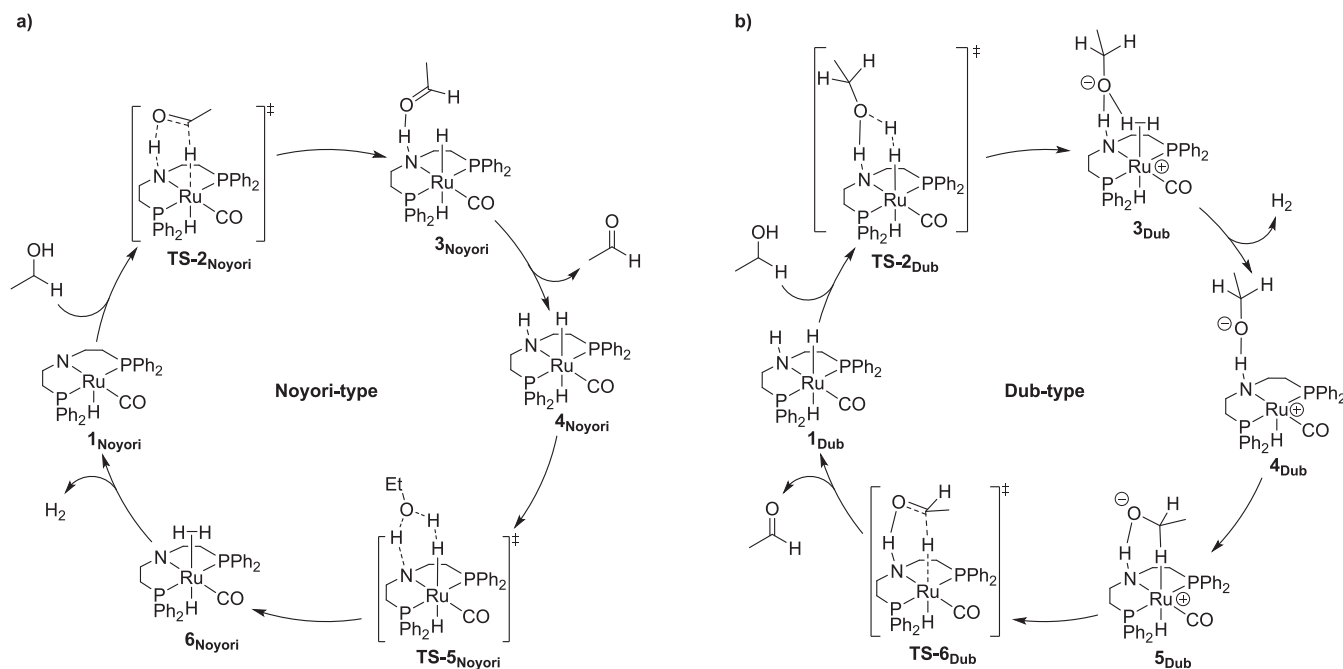
Rationalization of the Observed Chemoselectivities.

To gain a deeper understanding of the underlying principles, the experimentally observed ruthenium species and their stoichiometric reactions with alcohols were investigated initially. First, the chosen quantum-chemical approach was validated by comparing the calculated structures of **5** and **6** with their molecular structures in the solid state (Tables S4–S7). The Ru^{II} complex **5_{calc}** is found to be significantly more stable than the isomeric Ru⁰ complex (**5-iso_{calc}**; $\Delta G^{298} = 10.2 \text{ kJ mol}^{-1}$; Scheme 4a), while the computed relative energies of the PPh₃ counterparts (**6_{calc}** and **6-iso_{calc}**) indicate an endergonic Ru⁰-to-Ru^{II} isomerization ($\Delta G^{298} = 28.8 \text{ kJ mol}^{-1}$; Scheme 4b). Multiple contributions can be described that lead to a difference in the observed products when employing PMe₃ or PPh₃. First, the change from an octahedral to a trigonal-bipyramidal coordination geometry leads to a significant steric relaxation. Second, the more electron-rich Ru⁰ motif is favored by less electron-rich phosphine [Tolman electronic parameter: 2064 cm^{-1} (PMe₃) and 2069 cm^{-1} (PPh₃)].³⁶ Third, **6_{calc}** exhibits an N–H $\cdots\pi$ -phenyl interaction (Ru1–P3–C71, 111.8 $^\circ$), which was also identified in the crystal structure [Ru1–P3–C71, 113.8(3) $^\circ$] and increases the stability of this isomer (vide supra).

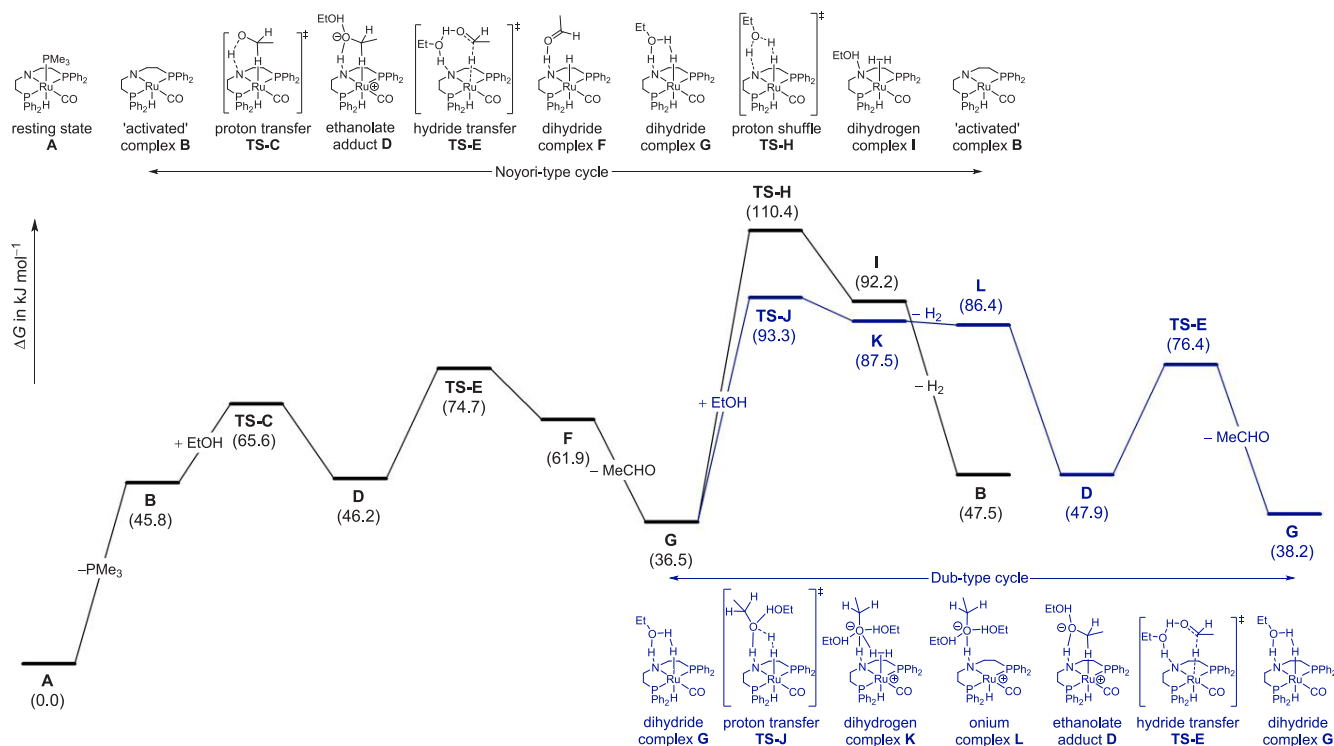
Next, the experimentally observed difference in the reactivity of **5** and **6** toward PhOH was probed by calculating the corresponding phenolato (**8-iso_{calc}** and **9_{calc}**, respectively) and onium (**8_{calc}** and **9-iso_{calc}**, respectively; Scheme 4c,d) complexes. The calculations show that protonation of **5_{calc}** leads to the very stable onium complex **8_{calc}** ($\Delta G^{298} = -40.4 \text{ kJ mol}^{-1}$), which is not prone to PMe₃ substitution through PhO[−], because this would lead to a species of higher relative energy (**8-iso_{calc}**; $\Delta G^{298} = 11.1 \text{ kJ mol}^{-1}$; Scheme 4c). Once more, the reactivity changes when PPh₃ is employed: a more stable ruthenium(II) phenolato complex is observed (Scheme 4d; **9_{calc}**; $\Delta G^{298} = 8.1 \text{ kJ mol}^{-1}$; **9-iso_{calc}**; $\Delta G^{298} = 10.0 \text{ kJ mol}^{-1}$). Although the difference in free energy between **9_{calc}** and **9-iso_{calc}** ($\Delta \Delta G^{298} = 1.9 \text{ kJ mol}^{-1}$) is far much smaller than that between **8-iso_{calc}** and **8_{calc}** ($\Delta \Delta G^{298} = 51.5 \text{ kJ mol}^{-1}$), it should be noted that the free-energy difference will increase because of the entropically unfavored phenolato complex **9-iso_{calc}** at higher reaction temperatures. A loss in entropy would be expected because of the conversion of two molecules (**5_{calc}** + PhOH or **6_{calc}** + PhOH) to a tightly coupled ion pair (**8_{calc}** or **9-iso_{calc}**, respectively) rather than in the formation of **8-iso_{calc}** or **9_{calc}** in which the number of molecules remains unchanged. Similar to the discussed energetic differences of **5** and **6**, the inverted stability is attributed to the different substituents of the phosphine ligands. The onium complex will be preferred if the PR₃ ligand is not too sterically demanding. This renders the octahedral coordination environment, in which PR₃ is bound to the Ru center, more feasible, and provides additional space for a stabilizing hydrogen bond between the alcoholate anion and the complex. The higher steric demand of PPh₃ does not favor the structure of **9-iso_{calc}** but rather PPh₃ substitution by the phenolato becomes preferred (Scheme 4d). This also offers an explanation for the observed energy difference between **8_{calc}** and **9-iso_{calc}** ($\Delta \Delta G^{298} = 50.4 \text{ kJ mol}^{-1}$) in contrast to the small difference in energy of formation between **8-iso_{calc}** and **9_{calc}** ($\Delta \Delta G^{298} = 3.0 \text{ kJ mol}^{-1}$).

Computational Investigation of the Reaction Mechanism. Complexes **5** and **6** have been shown to lead to closely related species upon reaction with alcohols. Therefore, the possibility of different mechanistic scenarios for each of the complexes was investigated. The literature is coined by the

Scheme 5. Catalytic Cycles for the Dehydrogenation of Ethanol to Ethanal Catalyzed by a Ru-PNP Complex Analogously to the Proposed Mechanisms by (a) Noyori et al. and (b) Dub et al.



Scheme 6. Noyori- (Black) and Dub-Type (Blue) Lowest-Energy Pathways for the Dehydrogenation of Ethanol to Ethanal with Complex A (i.e., 5)^{4a}

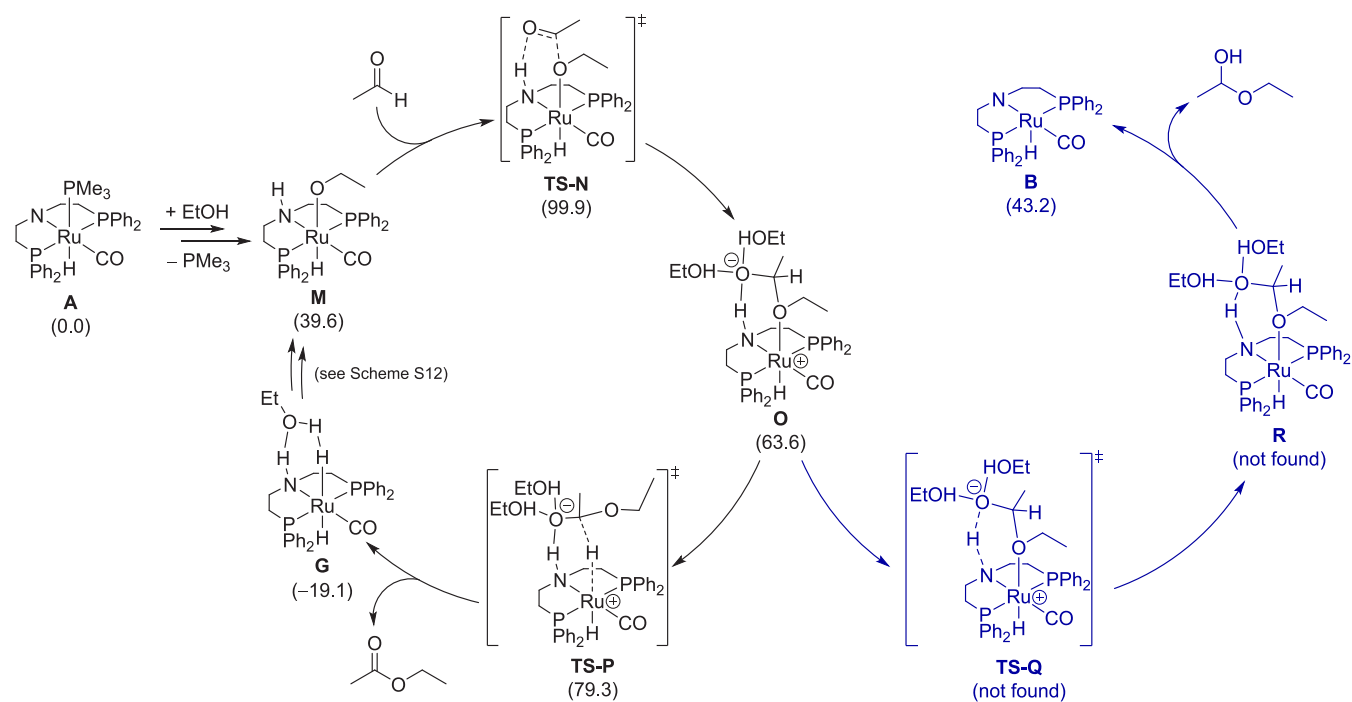


^{4a}Mass balance for additional stabilizing substrate equivalents is ensured in the entire scheme. ΔG^{383} in kJ mol^{-1} ; RI-PBE0-D3(BJ)/def2-QZVPP//BP86/def2-SV(P); COSMO-RS (toluene).

Noyori-type catalytic cycle (Scheme 5a), which enables (de)hydrogenation via metal–ligand cooperation (MLC).^{28a,37} More recently, Dub et al.^{28a,33,38} as well as others^{4c,39} have proposed a revised mechanism, which does not involve MLC (i.e., cleavage and formation of the N–H bond)

but rather a metal–ligand-assisted (MLA) pathway, in which N–H cleavage does not occur (Scheme 5b). In addition to these well-established mechanistic regimes, our computational investigations also included other mechanistic scenarios, of which some find precedence in the literature (see the Supporting

Scheme 7. Tishchenko-like Pathway Directly Generating Ethyl Acetate from Ethanol and Ethanal (Black) and Formation of Intermediary Hemiacetal for Further Dehydrogenation to the Desired Ester (Blue)^a



^aThe fate of complex **G** (e.g., how it can be converted to complex **M**) is discussed in detail in the [Supporting Information](#). Mass balance for additional stabilizing substrate equivalents is ensured in the entire scheme. ΔG^{383} in kJ mol^{-1} ; RI-PBE0-D3(BJ)/def2-QZVPP//BP86/def2-SV(P); COSMO-RS (toluene).

[Information](#)).⁴⁰ For all computed catalytic cycles, ethanol was employed as a substrate, which was also shown to be converted to ethyl acetate (see the [Supporting Information](#)). The application of Noyori's mechanism to the Ru-MACHO system leads to a cycle that proceeds from the conventionally proposed dehydrochlorinated Ru-MACHO ($\mathbf{I}_{\text{Noyori}}$) via a concerted proton hydride transfer (**TS-2_{Noyori}**) and the aldehyde adduct $\mathbf{3}_{\text{Noyori}}$ to the dihydride complex $\mathbf{4}_{\text{Noyori}}$ ([Scheme 5a](#)). This species undergoes an alcohol-assisted proton shuffle (**TS-5_{Noyori}**), which yields the ruthenium dihydrogen complex $\mathbf{6}_{\text{Noyori}}$, which subsequently liberates H_2 to regenerate $\mathbf{I}_{\text{Noyori}}$. The proton shuffling step is sometimes described as a direct proton transfer from the NH function to the metal center. However, calculations show that the explicit involvement of alcohol drastically lowers the activation barrier.^{28d,32} In contrast, applying Dub's mechanism to the Ru-MACHO system results in a different catalytic cycle: starting from the common species of both cycles, the ruthenium dihydride complex $\mathbf{1}_{\text{Dub}}$, a proton transfer from ethanol (**TS-2_{Dub}**) will yield complex $\mathbf{3}_{\text{Dub}}$, which subsequently liberates H_2 to form complex $\mathbf{4}_{\text{Dub}}$. The formation of an intramolecular C–H...Ru interaction (**S_{Dub}**) sets the stage for a hydride transfer (**TS-6_{Dub}**), ultimately leading to ethanal and the dihydride complex $\mathbf{1}_{\text{Dub}}$.

Although many mechanistic scenarios were evaluated in this study, our computational studies did not result in any feasible mechanistic regime in which the PR_3 ligand stays coordinated to the metal (see [Scheme S6](#) for details). Therefore, the only energetic difference between **5** and **6** results from the relative energy of the "activated" complex $\mathbf{1}_{\text{Noyori}}$ to the resting states, $\mathbf{5}_{\text{calc}}$ and $\mathbf{6}_{\text{calc}}$. The dissociation of PMe_3 in $\mathbf{5}_{\text{calc}}$ ($\Delta G^{383} = 45.8 \text{ kJ mol}^{-1}$) is 3.0 kJ mol^{-1} less favorable than the generation of **B** ([Scheme 6](#); cf. $\mathbf{1}_{\text{Noyori}}$) from $\mathbf{6}_{\text{calc}}$ ($\Delta G^{383} = 42.8 \text{ kJ mol}^{-1}$).

Therefore, only the catalytic cycles involving complex $\mathbf{5}_{\text{calc}}$ are discussed here (the analogous discussion for complex $\mathbf{6}_{\text{calc}}$ is provided in the [Supporting Information](#)). Starting from the Ru^{II}- PMe_3 complex (**A**), phosphine dissociation is endergonic ($\Delta G^{383} = 45.8 \text{ kJ mol}^{-1}$) and contributing significantly to the overall activation barrier. A cascade of proton (**TS-C**; $\Delta G^\ddagger = 65.6 \text{ kJ mol}^{-1}$) and hydride (**TS-E**; $\Delta G^\ddagger = 74.7 \text{ kJ mol}^{-1}$) transfers leads to **G**, which resembles the ethanol-stabilized equivalent of the dihydride complex $\mathbf{4}_{\text{Noyori}}$ (cf. [Scheme 5a](#)). Proton shuffle via **TS-H** ($\Delta G^\ddagger = 110.4 \text{ kJ mol}^{-1}$) leads to the dihydrogen complex **I** ($\Delta G^{383} = 92.2 \text{ kJ mol}^{-1}$), which regenerates the "activated" complex **B** ($\Delta G^{383} = 47.5 \text{ kJ mol}^{-1}$) after H_2 liberation and closes the Noyori-type cycle (cf. [Scheme 5a](#)). In contrast, the Dub-type pathway starts from dihydride complex **G** and results in complex **K** ($\Delta G^{383} = 87.5 \text{ kJ mol}^{-1}$) via proton transfer in **TS-J** ($\Delta \Delta G^{383} = 93.3 \text{ kJ mol}^{-1}$). Subsequent dihydrogen dissociation gives **L** ($\Delta G^{383} = 86.4 \text{ kJ mol}^{-1}$), and a highly exergonic formation of a C–H...Ru interaction leads to **D** ($\Delta G^{383} = 47.9 \text{ kJ mol}^{-1}$). Complex **D** liberates the product ethanal and regenerates the dihydride species **G** via an ethanol-assisted hydride transfer **TS-E** ($\Delta G^\ddagger = 76.4 \text{ kJ mol}^{-1}$).

In conclusion, the Dub-type MLA cycle was calculated to be significantly more favored over the Noyori-type metal–ligand cooperative process ($\Delta \Delta G^\ddagger = 17.1 \text{ kJ mol}^{-1}$). The rate-determining step in the Noyori- and Dub-type pathways is generation of the ruthenium dihydrogen complexes **I** (via **TS-H**) and **K** (via **TS-J**), respectively. However, because the ruthenium dihydride complex **G** must be formed from the resting state **A**, the initial sequence $\mathbf{A} \rightarrow \mathbf{B} \rightarrow \mathbf{D} \rightarrow \mathbf{F} \rightarrow \mathbf{G}$ of the Noyori-type cycle will be required to form the on-cycle species **G** for the Dub-type pathway. All alternative mechanisms

investigated during this study show higher Gibbs free energies of activation compared to the reaction pathways discussed above (Scheme 6). Only one catalytic cycle based on the work by Hasanayn et al.^{40a} poses an alternative way to generate the ruthenium dihydride complex **G** via a “slippage” of the alcoholato ligand and is quite competitive to the Noyori-type pathway ($\Delta\Delta G^\ddagger = 5.5 \text{ kJ mol}^{-1}$; cf. Scheme S5). Although the activation barrier of the “slippage” mechanism is higher for our system, this could be a viable pathway for the formation of an on-cycle species of the energetically favored Dub-type cycle and should be considered in the investigation of similar systems.

For the Dub-type cycle, the resting state **A** can again be accessed through the sequence $\text{D} \rightarrow \text{B} \rightarrow \text{A}$ (i.e., to the reverse sequence in the Noyori-type cycle) because the barrier of TS-C ($\Delta G^\ddagger = 65.6 \text{ kJ mol}^{-1}$; Scheme 6) is far more feasible than regenerating the dehydrochlorinated Ru-MACHO (**B**) directly from the dihydride complex **G** (via TS-H; $\Delta G^\ddagger = 110.4 \text{ kJ mol}^{-1}$).

Furthermore, the original in the Noyori-type cycle proposing concerted proton hydride transfer (TS-2_{Noyori}; Scheme 5a) could not be located.^{37a} A stepwise pathway $\text{B} \rightarrow \text{F}$ via TS-C, **D**, and TS-E (Scheme 6) will perform the same transformation at a feasible activation barrier ($\Delta G^\ddagger = 74.7 \text{ kJ mol}^{-1}$). This phenomenon has been discussed previously and was attributed to the choice of solvent modeling.^{10j,28a} Moreover, Dub et al. highlighted that there is a significant difference in the calculated energies depending on their choice of solvent modeling.^{28a} A similar observation was made when looking at stabilization of the rate-determining steps (TS-J and TS-H) by one or two additional substrate molecules. The use of explicit ethanol stabilization, which means to specifically calculate the system with the ethanol molecules rather than just using COSMO-RS or a similar approximation method, always leads to the MLA pathway (TS-J). In particular, this transition state could not be characterized without such interactions, while TS-H could only be located without including any further substrate molecules in the calculations. This agrees with the chemical intuition that stabilization of the anionic fragment would significantly decrease its tendency to abstract the N–H proton.

After alcohol dehydrogenation to an aldehyde, two different pathways for ester formation will compete:^{28b} On the one hand, a Tishchenko-like coupling of one molecule of each, alcohol and aldehyde, at the metal center to the ester could occur. On the other hand, intermediary hemiacetal formation in combination with a second dehydrogenation step would also yield the ester product (Scheme 7). Each of these pathways have been previously suggested to take part in these types of reactions.^{2a,28b,c} Both share the initial transition state TS-N to form species **O** ($\Delta G^{383} = 63.6 \text{ kJ mol}^{-1}$) from the ethanolato complex **M** ($\Delta G^{383} = 39.6 \text{ kJ mol}^{-1}$) via an activation barrier of 99.9 kJ mol^{-1} . Hydride transfer (TS-P) will break down complex **O** into the dihydride complex **G** and ethyl acetate ($\Delta G^\ddagger = 79.3 \text{ kJ mol}^{-1}$). On the contrary, TS-Q would transform complex **O** to the hemiacetal adduct **R**. This as well as a one-step transformation from **O** to **B** could not be located. Geometry optimizations repeatedly led back to complex **O**, indicating that these are higher in energy. Last, the transition state for the metal-free hemiacetal formation was calculated and found to be kinetically disfavored ($\Delta G^\ddagger = 110.8 \text{ kJ mol}^{-1}$; Scheme S11). Consequently, the observations indicate that the ester is directly formed on the metal complex without the hemiacetal being released as an intermediate.

Probing the Catalysts’ Stabilities. As shown in the previous section, Ru-MACHO (**1a**)/base, **5**, and **6** serve as precatalysts for the same catalytic cycle after activation (i.e., base-induced HCl abstraction or PR_3 dissociation/substitution). Because the initial goal of this work was to stabilize the “activated” Ru-MACHO (**2**) and prevent its decomposition, the next step was to test whether complexes **5** and **6** show a stability advantage over the Ru-MACHO/base system. Because **5** and **6** showed essentially the same catalytic performance, the focus in these experiments was put on complex **6** with its PPh_3 ligand because PPh_3 is much easier to handle on both a laboratory and an industrial scale: PPh_3 is an odorless and cheap bulk chemical as opposed to the much more expensive, air-sensitive, and toxic PMe_3 with its strongly unpleasant odor, which would be especially of relevance in the synthesis of esters used as fragrances.

It was noticed early in this study that the gas chromatograms of the reaction mixtures looked quite different depending on the catalytic system employed (see the Supporting Information): in the case of Ru-MACHO (**1a**) and KOtBu (a 100-fold excess with respect to **1a** was used; this typical Ru-MACHO/base ratio was used in many other reports), several other unassigned signals besides the expected ones for solvents, tBuOH (from the base KOtBu), and the ester product were detected (Figure S30). A much cleaner gas chromatogram was obtained in the reaction catalyzed by **6** (Figure S31). In line with the previous observation that Ru-MACHO (**1a**) can be decomposed in the presence of strong bases (cf. Scheme 1), it is suggested that the additional signals in the gas chromatogram belong to species formed by catalyst degradation and/or unwanted side reactions. A similar observation was made when complex **6** was employed in a catalytic dehydrogenation in the presence of a 100-fold excess of KOtBu (Figure S32). This finding is further supported by the positive-ion electrospray ionization (ESI+) mass spectra of the three reaction mixtures after completion and removal of all volatiles in vacuo (Figure 5). The mass spectrum of the reaction catalyzed by **6** shows essentially only one major signal (m/z 832.1606), which is assigned to the $[\text{6} - \text{H}]^+$ ion (Figure 5a; see also Figure S36 for the isotope pattern). In contrast, the mass spectrum of the reaction catalyzed by Ru-MACHO (**1a**)/ KOtBu shows no signal for the dehydrochlorinated Ru-MACHO, which is usually observed as $[\text{2} + \text{H}]^+$ (m/z 572.08).^{17,18} Instead, several signals in the mass range m/z 700–1200 were detected that cannot be assigned to any plausible structures at the moment (Figure 5b). It shows a pattern similar to that of the spectrum recorded of the base-induced, but substrate-free, decomposition of Ru-MACHO (**1a**, Figure S35). The reaction catalyzed by **6** with an excess of KOtBu gave a mass spectrum with multiple signals (range: m/z 700–1200) of which one (m/z 832.1606) matched again the expected mass of the $[\text{6} - \text{H}]^+$ ion (Figure 5c). In addition, the in situ generation of **6** was also investigated by employing catalytic amounts of Ru-MACHO (**1a**, 1.0 equiv), KOtBu (1.0 equiv), and PPh_3 (3.0 equiv). The results of mass spectrometric analyses are similar to those obtained with isolated complex **6** (Figures S37 and S38), proving that isolation of the stabilized dehydrochlorinated Ru-MACHO is not a requirement to obtain a catalytically active system with an improved stability.

The avoided decomposition of the “activated” Ru-MACHO (**2**) in the presence of PPh_3 was expected to be reflected in the turnover numbers (TONs) of the two catalytic systems. To test this, dehydrogenative coupling reactions were conducted with purified hexanol and toluene at low catalyst loadings with a 1:1

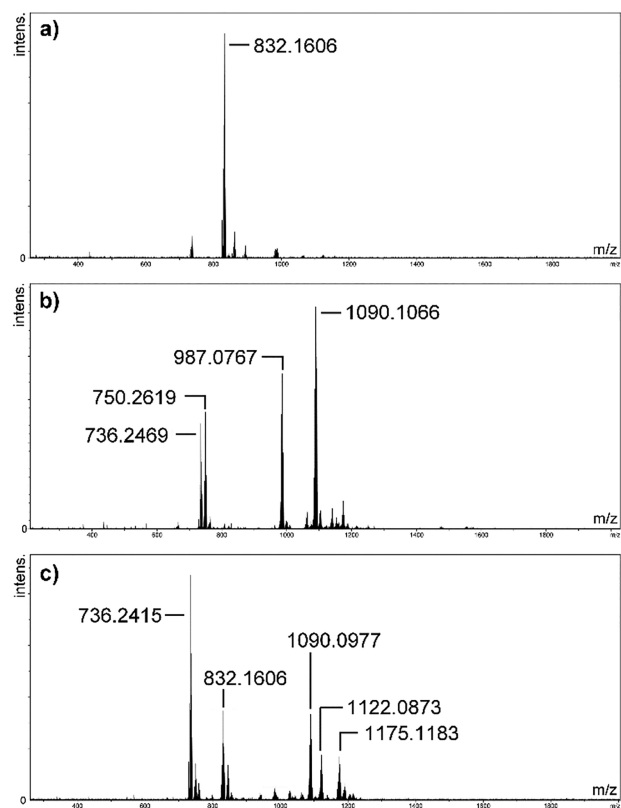


Figure 5. ESI+ mass spectra (mass range: m/z 200–2000) recorded after the evaporation of all volatiles in vacuo. Reaction conditions (all 5 mmol of hexanol in refluxing toluene overnight): (a) 0.12 mol % **6**; (b) 0.14 mol % Ru-MACHO (**1a**) and 10 mol % KOtBu; (c) 0.13 mol % **6** and 10 mol % KOtBu.

ratio of Ru-MACHO (**1a**) and KOtBu with and without a 13-fold excess of PPh₃. At S/C = 32500, a 37% conversion (>99% selectivity) of the alcohol to the ester was obtained for both catalytic systems. This corresponds to a TON of 12000 and is in the range of what is reported in the literature (note that, for example, the reported TON of 15400 was obtained at a **1a**-to-base ratio of 1:120^{6b}). This indicates that, as long as enough substrate is available, the catalytic system cannot benefit from the stabilizing effect of the phosphine. Therefore, this effect should be observed in batchwise reactions, where the catalyst is recycled. Because such a recycling is challenging for an air-sensitive, homogeneous catalyst on a laboratory scale, we decided to measure the initial rate kinetics of three consecutive dehydrogenations as a sensitive probe for catalyst deactivation.⁴¹ In this catalyst recycling experiment, a batch of hexanol (10 mmol; S/C = 670) was added to the refluxing reaction mixture after 3 and 6 h (see the Supporting Information for experimental details). Here, it is important that the first batch of hexanol was already fully consumed after less than 1 h for each of the catalytic systems [Ru-MACHO/KOtBu (1:1) and **6**]. Hence, the catalysts were left without substrate for >2 h at 110 °C. In the first batch, the rate of the Ru-MACHO/base system [$-k_1(\mathbf{1a}/\text{KOtBu}) = (130 \pm 20) \times 10^{-5} \text{ s}^{-1}$] and the rate for complex **6** [$-k_1(\mathbf{6}) = (113 \pm 7) \times 10^{-5} \text{ s}^{-1}$] are the same within the experimental error. The preservation of the initial rates in the second and third batches with respect to the first batch was ca. 15% and 10% for **1a**/KOtBu and ca. 37% and 19% for **6** (Figure 6). This is a drastic drop in activity for both systems; however, the stabilized complex **6** exhibits almost the doubled rate of **1a**/

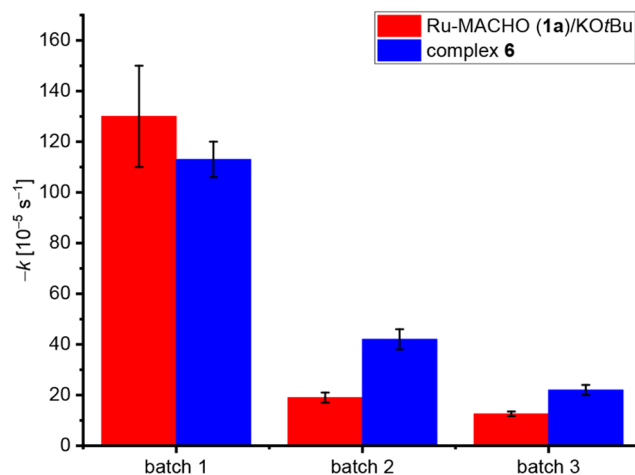


Figure 6. Column plot of the initial rates ($-k$) of three consecutive dehydrogenative couplings of hexanol catalyzed by Ru-MACHO (**1a**)/KOtBu (red) and complex **6** (blue).

KOtBu in the third batch ($-k_3$ in 10^{-5} s^{-1} : **1a**/KOtBu, 12.6 ± 0.9 ; **6**, 22 ± 2). These data, together with the MS measurements, are believed to exemplify that an appreciable stability advantage of the Ru-MACHO/base system can be achieved upon the addition of a phosphine. Consequently, further studies are required to render this approach applicable.

In summary, these experiments show that 1 equiv of base is sufficient to generate **2**, while higher base loadings degrade the catalyst (cf. Figures 5c and S38). The catalyst is active as long as a substrate is available and suffers from deactivation the longer it is left without a suitable substrate. This can be opposed by adding a stabilizer (e.g., PPh₃) to the reaction mixture or using the stabilized “activated” Ru-MACHO (i.e., complexes **5** or **6**) directly if base-free conditions are necessary.

Role of the Base in Reactivating Deactivated Catalysts. It is unquestionable that only 1 equiv of base is necessary to dehydrochlorinate Ru-MACHO and its derivatives (**1a**–**1c**) to generate the activated catalyst **2**. Contrary to that, a brief look at the literature reveals that a large (i.e., up to a 100-fold) excess of base is usually employed in (de)hydrogenation reactions. As was shown, this excess leads to catalyst degradation, and only 1 equiv of base with respect to the catalyst is required if high-grade materials are used. Nguyen et al. have reported that one main deactivation pathway of **1b** occurs through traces of water, giving rise to catalytically inactive ruthenium carboxylate complexes, which have been shown to be reactivated by base.^{28c}

In the aforementioned dehydrogenative coupling of hexanol at low catalyst loadings (previous section), it was found that supplementing catalyst **6** with an equimolar amount of KOtBu improved the reaction outcome significantly (S/C = 32200, 49% conversion, TON = 16000). Even though great care was taken in the purification of the starting materials, small amounts of impurities seem to have a major impact on the reaction outcome. Consequently, accurate comparisons between different systems can only be made if the amount of base is kept constant.

Briefly, the nature of deactivation species derived from **5** and **6** was also investigated. Benzoic acid was chosen as an archetypical deactivating agent and reacted in a 1:1 molar ratio with **5** as well as **6**. The former was simply protonated at the amido nitrogen (Scheme 8), and the resulting onium complex **12** resembles spectroscopic and structural features very similar to those described earlier for complex **8** (Figure 7). The complex'

Scheme 8. Reactions of 5 and 6 with Benzoic Acid

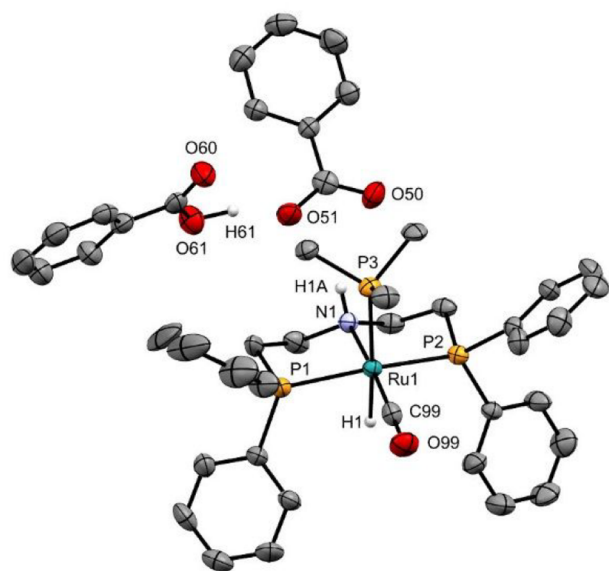
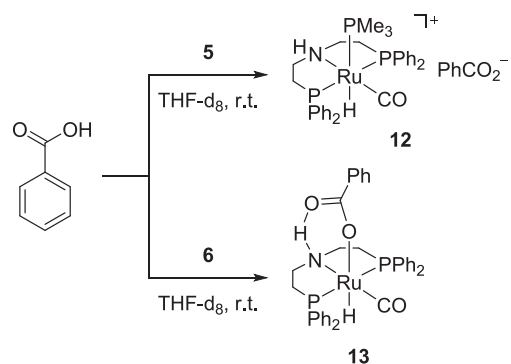


Figure 7. Molecular structure of **12** in the solid state with ellipsoids depicted at the 50% probability level. C–H hydrogen atoms are omitted for clarity. Selected distances (Å) and angles (deg): Ru1–C99, 1.832(5); Ru1–N1, 2.193(4); Ru1–P1, 2.318(2); Ru1–P2, 2.327(2); Ru1–P3, 2.436(2); Ru1–H1, 1.69(4); C99–Ru1–N1, 172.9(2); C99–Ru1–P1, 95.7(2); C99–Ru1–P2, 97.2(2); C99–Ru1–P3, 95.9(2); C99–Ru1–H1, 89(2); N1–Ru1–P3, 91.2(2); N1–Ru1–H1, 84(2); P1–Ru1–P2, 160.05(5); P1–Ru1–P3, 97.04(5); P2–Ru1–P3, 96.73(4); P3–Ru1–H1, 175(2).

benzoate counteranion interacts with the NH functionality of the onium complex and a cocrystallized molecule of benzoic acid through hydrogen bonding [N1–O50, 3.272(5) Å; N1–O51, 3.062(5) Å; O51–O61, 2.506(5) Å].

The latter (**6**), in contrast, exhibited reactivity toward benzoic acid similar to that observed toward PhOH earlier (*vide supra*). The Ru⁰ center is protonated [$\delta_{\text{H}} = -17.00$ ppm (t, $J = 19.7$ Hz)] and PhCO₂[−] substitutes the PPh₃ ligand [$\delta_{\text{P}} = 55.3$ (s), -5.5 (s) ppm] to furnish complex **13** (Scheme 8). Crystals suitable for X-ray diffraction analysis were grown by layering the NMR sample with pentane. Colorless crystals of two habits (some appeared as plates and others as planks) were found in the sample, and both were measured on the diffractometer. The colorless plates resulted in the expected structure of **13** (**13a**, Figure 8). The benzoate trans to the hydride H1 bridges the ruthenium center and the NH functionality via a hydrogen bond [N1–O50, 1.256(3) Å]. The spectroscopic and structural data match those of the literature-known formate and acetate

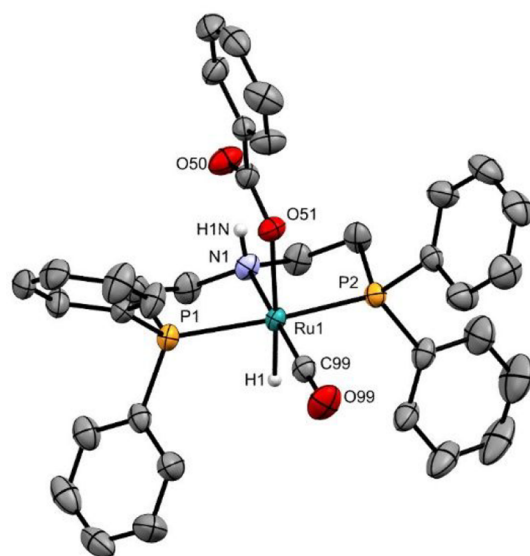
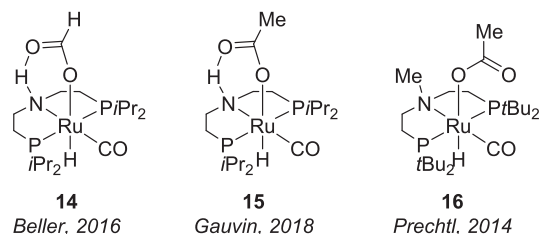


Figure 8. Molecular structure of **13a** in the solid state with ellipsoids depicted at the 50% probability level. C–H hydrogen atoms are omitted for clarity. Selected distances (Å) and angles (deg): Ru1–C99, 1.841(3); Ru1–N1, 2.184(2); Ru1–O51, 2.231(2); Ru1–P1, 2.3242(6); Ru1–P2, 2.3014(6); Ru1–H1, 1.57(2); C99–Ru1–N1, 174.2(1); C99–Ru1–O51, 96.71(9); C99–Ru1–P1, 100.34(8); C99–Ru1–P2, 94.53(8); C99–Ru1–H1, 88.0(8); N1–Ru1–O51, 88.45(8); N1–Ru1–H1, 87.0(8); O51–Ru1–P1, 94.31(5); O51–Ru1–P2, 90.87(5); P1–Ru1–P2, 163.55(2); O51–Ru1–H1, 175.0(9).

complexes derived from **1b** very well (**14**^{10j} and **15**,^{28c} respectively; Chart 2).

Chart 2. Structurally Described Literature-Known Complexes Related to **13a** and **13b**

Structure determination from the colorless planks, however, revealed a conformational polymorph of **13** with two independent molecules in the asymmetric unit (Figure 9; only one independent molecule is depicted). In the molecular structure, the hydride and NH hydrogen exhibit a *cis* orientation. Consequently, the envelope conformation of the two five-membered metallacycles is inverted compared to **13a**. Most obvious is the conformational difference around the Ru–O bond, which is *syn*-periplanar to the CO group rather than *anti*-periplanar as **13a** is [**13a**, C99–Ru1–O51–C50, 168.1(2)°; **13b**, C99–Ru1–O51–C50, 1.7(5)°, 2.4(5)°]. This conformation is only possible because the two independent molecules engage in an intermolecular hydrogen bond between the carbonyl oxygen and the NH hydrogen [N1–O50, 2.913(7) and 2.897(7) Å]. This leads to a polymeric chain throughout the crystal lattice (Figure S2). This structural feature has not been reported in the literature for these types of complexes. The most similar complex **16** (Chart 2) adopts the same *syn*-periplanar

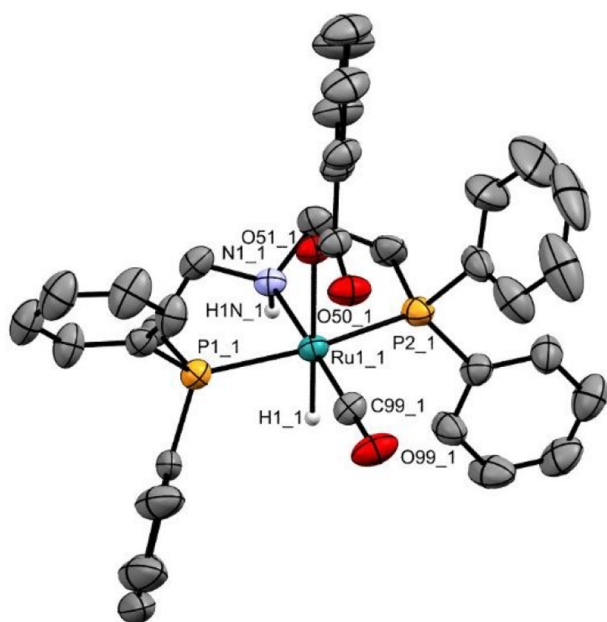


Figure 9. Molecular structure of **13b** in the solid state with ellipsoids depicted at the 50% probability level. C–H hydrogen atoms, the second independent molecule, and three molecules of cocrystallized THF are omitted for clarity. Selected distances (Å) and angles (deg): Ru1–C99, 1.815(6); Ru1–O51, 2.184(4); Ru1–N1, 2.195(5); Ru1–P2, 2.309(2); Ru1–P1, 2.311(2); Ru1–H1, 1.59(6); C99–Ru1–N1, 175.0(2); C99–Ru1–O51, 101.7(2); C99–Ru1–P1, 98.5(2); C99–Ru1–P2, 97.3(2); C99–Ru1–H1, 81(2); N1–Ru1–O51, 83.1(2); N1–Ru1–H1, 94(2); O51–Ru1–P1, 97.2(2); O51–Ru1–P2, 86.4(2); P1–Ru1–P2, 162.68(6); O51–Ru1–H1, 177(2).

conformation [C–Ru–O–C, 2.6(2)°] but cannot form the polymeric chains because the NH group is replaced by an NMe group.^{16b} Accordingly, the conformation of **16** is believed to be a result of the smaller steric clash between the acetate and NMe group.

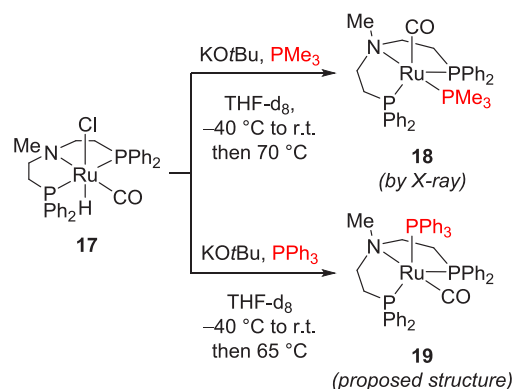
It was not surprising to find that both **12** and **13** did not lead to any ester formation in the catalytic dehydrogenation of hexanol. When a 3-fold excess of KOtBu (with respect to the catalysts) was added to the mixtures, the reaction proceeded smoothly at high conversions (>99%) and selectivities (>95%).

Attempts to Synthesize Other Ru⁰-PNP Complexes.

Looking at complex **6**, one might wonder if other Ru⁰ complexes bearing the aliphatic PNP ligand scaffold are accessible. Some preliminary experiments were conducted with the methylated Ru-MACHO complex **17**,^{9a} although knowing that it will probably not furnish competent (pre)catalysts for (de)hydrogenation reactions. Similar to the synthetic routes of **5** and **6** (vide supra), **17** was reacted with KOtBu in the presence of PMe₃ and PPh₃ in two separate NMR experiments (Scheme 9). In both experiments, no signals were observed below 0 ppm in the ¹H NMR spectra. In the ³¹P{¹H} NMR spectra of the reaction with PMe₃, a doublet (53.9 ppm, *J* = 32.9 Hz) and a triplet (23.6 ppm, *J* = 32.9 Hz) were detected, while the spectrum of the reaction with PPh₃ showed two apparent doublets of doublets (54.8 and 47.2 ppm), similar to those found in the formation of **6** (vide supra). Both experiments suggested the formation of the anticipated Ru⁰ complexes **18** and **19** (Scheme 9).

Unfortunately, the reactions turned out to be sluggish, and dedicated syntheses to obtain clean material for further studies have not been successful yet. However, it was possible to obtain

Scheme 9. Reactions toward Other Ru⁰ Complexes Derived from the Methylated Ru-MACHO (**17**)



crystals from the NMR experiment with PMe₃ by layering the NMR sample with pentane (Figure 10). Indeed, the molecular

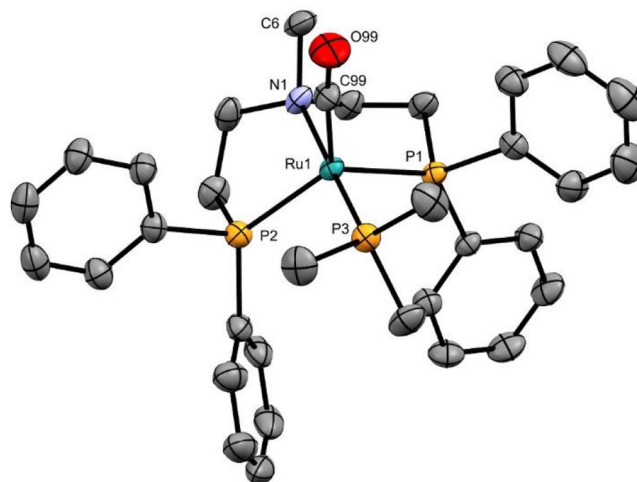


Figure 10. Molecular structure of **18** in the solid state with ellipsoids depicted at the 50% probability level. Hydrogen atoms and disordered ethylene bridges are omitted for clarity. Selected distances (Å) and angles (deg): Ru1–C99, 1.860(2); Ru1–N1, 2.262(2); Ru1–P1, 2.2895(4); Ru1–P2, 2.3127(4); Ru1–P3, 2.2566(5); C99–Ru1–N1, 92.85(7); C99–Ru1–P1, 113.73(5); C99–Ru1–P2, 125.24(5); C99–Ru1–P3, 87.56(6); N1–Ru1–P3, 179.06(4); P1–Ru1–P2, 119.77(2); P1–Ru1–P3, 95.695(15); P2–Ru1–P3, 97.78(2).

structure confirms the assumed formation of a pentacoordinated Ru⁰ complex ($\tau = 0.90^{26}$). While the PNP pincer ligand arranges in a comparable fashion around the metal center as in **6**, the positions of CO and phosphine are interchanged. Here, PMe₃ is located trans to the amine nitrogen [N1–Ru1–P3, 179.06(4)°], and CO is bound in the equatorial position next to the phosphine side arms [P1–Ru1–C99, 113.73(5)°; P2–Ru1–C99, 125.24(5)°]. As far as the literature is concerned, it seems that this is the first example of a Ru⁰-PNP complex, bearing a phosphine and a CO in this configuration. The closest representatives are, in fact, complexes **3** and **6**, whose trigonal-bipyramidal geometry features the trans arrangement of the ligands' nitrogen and CO [Ru–N distances: **3**, 2.25(1) Å; **6**, 2.246(6) Å; **18**, 2.262(2) Å].

The first catalytic experiments with **18** (75% purity by ³¹P{¹H} NMR spectroscopy) and in situ generated **19** did not show any significant conversion in the dehydrogenative coupling

of hexanol. This agrees with the literature and our calculations: the presence of the NH group is the important feature to obtain an effective catalyst, and the nature of the Ru⁰ center does not change the operating mechanism.

SUMMARY AND CONCLUSION

This work shows that the previously reported degradation of Ru-MACHO (**1a**) by a base can be prevented to a certain extent by adding a phosphine, which stabilizes the “activated” Ru-MACHO (**2**). The choice of phosphine influences the nature of the obtained complexes: while the small PMe₃ simply coordinates at the vacant site in the Ru^{II} complex **2** (resulting in complex **5**), the bulkier PPh₃ results in an isomeric, pentacoordinated Ru⁰ complex (**6**). Both isolated complexes showed a similar reactivity toward alcohols and esters at low catalyst loadings in the absence of a base. These observations could be rationalized by quantum-chemical calculations, which identified three factors determining the formation of the Ru^{II} versus Ru⁰ isomer: the steric bulk and electronic nature of the phosphine employed and a stabilizing N–H⋯π-phenyl interaction. Furthermore, it was shown that **5** and **6** are precatalysts to the same catalytic cycle after phosphine dissociation because no energetically feasible pathway was located that did not include phosphine dissociation. The system does not involve an on-cycle Ru⁰ species. The Ru⁰ complex **6** only serves as a rather unexpected resting state, which is converted—base-free—to the “activated” complex **2**, which is traditionally generated in situ from Ru-MACHO (**1a**) and a base. The thorough computational evaluation leads to the conclusion that the Dub-type mechanism poses the energetically most favored pathway for alcohol dehydrogenation to the corresponding aldehyde. A series of transition states that are characterized by stabilizing hydrogen bonds between the NH functionality and the substrate are the key aspect of this scenario (i.e., MLA mechanism). This contrasts the commonly proposed (Noyori-type) metal–ligand cooperative mechanism, which requires a reversible N–H bond cleavage and was found to be significantly less feasible ($\Delta\Delta G^\ddagger = 17.1 \text{ kJ mol}^{-1}$). The subsequent coupling of an aldehyde and an alcohol to the ester was identified to occur on the metal complex without interim generation of a free hemiacetal.⁴² A series of experiments provided evidence that the addition of a phosphine ligand could increase the lifetime of the defined Ru-PNP catalytic system after the reaction is complete. Finally, the catalyst’s performance can be fine-tuned by small amounts of base, which capture detrimental impurities and do not harm the catalyst much.

ASSOCIATED CONTENT

Supporting Information

The Supporting Information is available free of charge at <https://pubs.acs.org/doi/10.1021/acs.inorgchem.0c00337>.

Experimental details, computational details, NMR spectra, and Cartesian coordinates for the optimized structures (PDF)

Accession Codes

CCDC 1958129–1958137 contain the supplementary crystallographic data for this paper. These data can be obtained free of charge via www.ccdc.cam.ac.uk/data_request/cif, or by emailing data_request@ccdc.cam.ac.uk, or by contacting The Cambridge Crystallographic Data Centre, 12 Union Road, Cambridge CB2 1EZ, UK; fax: +44 1223 336033.

AUTHOR INFORMATION

Corresponding Author

Thomas Schaub — Catalysis Research Laboratory (CaRLa), D-69120 Heidelberg, Germany; BASF SE, Organic Synthesis, D-67056 Ludwigshafen, Germany; orcid.org/0000-0003-2332-0376; Email: thomas.schaub@basf.com

Authors

Daniel J. Tindall — Catalysis Research Laboratory (CaRLa), D-69120 Heidelberg, Germany

Maximilian Menche — Catalysis Research Laboratory (CaRLa), D-69120 Heidelberg, Germany; BASF SE, Quantum Chemistry & Molecular Simulation, D-67056 Ludwigshafen, Germany

Mathias Schelwies — BASF SE, Organic Synthesis, D-67056 Ludwigshafen, Germany

Rocco A. Paciello — BASF SE, Organic Synthesis, D-67056 Ludwigshafen, Germany

Ansgar Schäfer — BASF SE, Quantum Chemistry & Molecular Simulation, D-67056 Ludwigshafen, Germany

Peter Comba — Institute of Inorganic Chemistry & Interdisciplinary Center for Scientific Computing, Heidelberg University, D-69120 Heidelberg, Germany; orcid.org/0000-0001-7796-3532

Frank Rominger — Institute of Organic Chemistry, Heidelberg University, D-69120 Heidelberg, Germany

A. Stephen K. Hashmi — Catalysis Research Laboratory (CaRLa), D-69120 Heidelberg, Germany; Institute of Organic Chemistry, Heidelberg University, D-69120 Heidelberg, Germany; orcid.org/0000-0002-6720-8602

Complete contact information is available at:

<https://pubs.acs.org/10.1021/acs.inorgchem.0c00337>

Author Contributions

[†]These authors contributed equally. The manuscript was written through contributions of all authors. All authors have given approval to the final version of the manuscript.

Notes

The authors declare no competing financial interest.

ACKNOWLEDGMENTS

The authors thank the analytical departments of the Organisch-Chemisches Institut for excellent support. CaRLa is cofinanced by the Ruprecht-Karls-Universität Heidelberg (Heidelberg University) and BASF SE.

REFERENCES

- (1) (a) de Vries, J. G. *The Handbook of Homogeneous Hydrogenation*; Wiley-VCH: Weinheim, Germany, 2007. (b) Ager, D. J.; de Vries, A. H. M.; de Vries, J. G. Asymmetric homogeneous hydrogenations at scale. *Chem. Soc. Rev.* **2012**, *41*, 3340–3380. (c) Clarke, M. L. Recent developments in the homogeneous hydrogenation of carboxylic acid esters. *Catal. Sci. Technol.* **2012**, *2*, 2418–2423. (d) Dub, P. A.; Ikariya, T. Catalytic Reductive Transformations of Carboxylic and Carbonic Acid Derivatives Using Molecular Hydrogen. *ACS Catal.* **2012**, *2*, 1718–1741. (e) Werkmeister, S.; Junge, K.; Beller, M. Catalytic Hydrogenation of Carboxylic Acid Esters, Amides, and Nitriles with Homogeneous Catalysts. *Org. Process Res. Dev.* **2014**, *18*, 289–302. (f) Pritchard, J.; Filonenko, G. A.; van Putten, R.; Hensen, E. J. M.; Pidko, E. A. Heterogeneous and homogeneous catalysis for the hydrogenation of carboxylic acid derivatives: history, advances and future directions. *Chem. Soc. Rev.* **2015**, *44*, 3808–3833. (g) Saudan, L. A. Hydrogenation of Esters. In *Applied Homogeneous Catalysis with Organometallic Compounds: A Comprehensive Handbook in Four*

Volumes, 3rd ed.; Cornils, B., Herrmann, W. A., Beller, M., Paciello, R., Eds.; Wiley-VCH: Weinheim, Germany, 2017; pp 645–680.

(2) (a) Zhang, J.; Leitus, G.; Ben-David, Y.; Milstein, D. Facile Conversion of Alcohols into Esters and Dihydrogen Catalyzed by New Ruthenium Complexes. *J. Am. Chem. Soc.* **2005**, *127*, 10840–10841. (b) Zhang, J.; Leitus, G.; Ben-David, Y.; Milstein, D. Efficient Homogeneous Catalytic Hydrogenation of Esters to Alcohols. *Angew. Chem., Int. Ed.* **2006**, *45*, 1113–1115.

(3) For a selection of systems that have been reported to have TONs > 10000, see: (a) Saudan, L. A.; Saudan, C. M.; Debieux, C.; Wyss, P. Dihydrogen Reduction of Carboxylic Esters to Alcohols under the Catalysis of Homogeneous Ruthenium Complexes: High Efficiency and Unprecedented Chemoselectivity. *Angew. Chem., Int. Ed.* **2007**, *46*, 7473–7476. (b) Spasyuk, D.; Gusev, D. G. Acceptorless Dehydrogenative Coupling of Ethanol and Hydrogenation of Esters and Imines. *Organometallics* **2012**, *31*, 5239–5242. (c) Spasyuk, D.; Smith, S.; Gusev, D. G. Replacing Phosphorus with Sulfur for the Efficient Hydrogenation of Esters. *Angew. Chem., Int. Ed.* **2013**, *52*, 2538–2542. (d) Li, W.; Xie, J.-H.; Yuan, M.-L.; Zhou, Q.-L. Ruthenium complexes of tetradentate bipyridine ligands: highly efficient catalysts for the hydrogenation of carboxylic esters and lactones. *Green Chem.* **2014**, *16*, 4081–4085. (e) Filonenko, G. A.; Aguila, M. J. B.; Schulpen, E. N.; van Putten, R.; Wiecko, J.; Müller, C.; Lefort, L.; Hensen, E. J. M.; Pidko, E. A. Bis-N-heterocyclic Carbene Aminopincer Ligands Enable High Activity in Ru-Catalyzed Ester Hydrogenation. *J. Am. Chem. Soc.* **2015**, *137*, 7620–7623. (f) Spasyuk, D.; Vicent, C.; Gusev, D. G. Chemoselective Hydrogenation of Carbonyl Compounds and Acceptorless Dehydrogenative Coupling of Alcohols. *J. Am. Chem. Soc.* **2015**, *137*, 3743–3746. (g) Tan, X.; Wang, Q.; Liu, Y.; Wang, F.; Lv, H.; Zhang, X. A new designed hydrazine group-containing ruthenium complex used for catalytic hydrogenation of esters. *Chem. Commun.* **2015**, *51*, 12193–12196. (h) Tan, X.; Wang, Y.; Liu, Y.; Wang, F.; Shi, L.; Lee, K.-H.; Lin, Z.; Lv, H.; Zhang, X. Highly Efficient Tetradentate Ruthenium Catalyst for Ester Reduction: Especially for Hydrogenation of Fatty Acid Esters. *Org. Lett.* **2015**, *17*, 454–457.

(4) (a) Kuriyama, W.; Matsumoto, T.; Ogata, O.; Ino, Y.; Aoki, K.; Tanaka, S.; Ishida, K.; Kobayashi, T.; Sayo, N.; Saito, T. Catalytic Hydrogenation of Esters. Development of an Efficient Catalyst and Processes for Synthesising (R)-1,2-Propanediol and 2-(l-Menthoxy)-ethanol. *Org. Process Res. Dev.* **2012**, *16*, 166–171. (b) Lazzari, D.; Cassani, M. C.; Bertola, M.; Moreno, F. C.; Torrente, D. Homogeneous catalytic hydrogenation of perfluoro methyl esters. *RSC Adv.* **2013**, *3*, 15582–15584. (c) Otsuka, T.; Ishii, A.; Dub, P. A.; Ikariya, T. Practical Selective Hydrogenation of α -Fluorinated Esters with Bifunctional Pincer-Type Ruthenium(II) Catalysts Leading to Fluorinated Alcohols or Fluoral Hemiacetals. *J. Am. Chem. Soc.* **2013**, *135*, 9600–9603. (d) Ziebart, C.; Jackstell, R.; Beller, M. Selective Catalytic Hydrogenation of Diethyl Oxalate and Related Esters. *ChemCatChem* **2013**, *5*, 3228–3231. (e) Kim, S. H.; Hong, S. H. Transfer Hydrogenation of Organic Formates and Cyclic Carbonates: An Alternative Route to Methanol from Carbon Dioxide. *ACS Catal.* **2014**, *4*, 3630–3636. (f) Fairweather, N. T.; Gibson, M. S.; Guan, H. Homogeneous Hydrogenation of Fatty Acid Methyl Esters and Natural Oils under Neat Conditions. *Organometallics* **2015**, *34*, 335–339. (g) Gao, S.; Tang, W.; Zhang, M.; Wang, C.; Xiao, J. Ru-MACHO-Catalyzed Highly Chemoselective Hydrogenation of α -Keto Esters to 1,2-Diols or α -Hydroxy Esters. *Synlett* **2016**, *27*, 1748–1752.

(5) Wei, Q.; Zhang, F.; Zhao, X.; Wang, C.; Xiao, J.; Tang, W. Ru-Catalyzed highly diastereoselective hydrogenation of N-tert-butylsulfanyl ketimines for the synthesis of aryl glycine derivatives. *Org. Biomol. Chem.* **2017**, *15*, 5468–5471.

(6) (a) Nielsen, M.; Kammer, A.; Cozzula, D.; Junge, H.; Gladiali, S.; Beller, M. Efficient Hydrogen Production from Alcohols under Mild Reaction Conditions. *Angew. Chem., Int. Ed.* **2011**, *50*, 9593–9597. (b) Nielsen, M.; Junge, H.; Kammer, A.; Beller, M. Towards a Green Process for Bulk-Scale Synthesis of Ethyl Acetate: Efficient Acceptorless Dehydrogenation of Ethanol. *Angew. Chem., Int. Ed.* **2012**, *51*, 5711–5713. (c) Nielsen, M.; Alberico, E.; Baumann, W.; Drexler, H.-J.; Junge, H.; Gladiali, S.; Beller, M. Low-temperature aqueous-phase methanol

dehydrogenation to hydrogen and carbon dioxide. *Nature* **2013**, *495*, 85–89. (d) Zhang, L.; Raffa, G.; Nguyen, D. H.; Swesi, Y.; Corbel-Demaiilly, L.; Capet, F.; Trivelli, X.; Desset, S.; Paul, S.; Paul, J.-F.; Fongarland, P.; Dumeignil, F.; Gauvin, R. M. Acceptorless dehydrogenative coupling of alcohols catalysed by ruthenium PNP complexes: Influence of catalyst structure and of hydrogen mass transfer. *J. Catal.* **2016**, *340*, 331–343.

(7) Oldenhuis, N. J.; Dong, V. M.; Guan, Z. Catalytic acceptorless dehydrogenations: Ru-Macho catalyzed construction of amides and imines. *Tetrahedron* **2014**, *70*, 4213–4218.

(8) Kothandaraman, J.; Czaun, M.; Goepfert, A.; Haiges, R.; Jones, J.-P.; May, R. B.; Prakash, G. K. S.; Olah, G. A. Amine-Free Reversible Hydrogen Storage in Formate Salts Catalyzed by Ruthenium Pincer Complex without pH Control or Solvent Change. *ChemSusChem* **2015**, *8*, 1442–1451.

(9) (a) Han, Z.; Rong, L.; Wu, J.; Zhang, L.; Wang, Z.; Ding, K. Catalytic Hydrogenation of Cyclic Carbonates: A Practical Approach from CO₂ and Epoxides to Methanol and Diols. *Angew. Chem., Int. Ed.* **2012**, *51*, 13041–13045. (b) Kothandaraman, J.; Goepfert, A.; Czaun, M.; Olah, G. A.; Surya Prakash, G. K. CO₂ capture by amines in aqueous media and its subsequent conversion to formate with reusable ruthenium and iron catalysts. *Green Chem.* **2016**, *18*, 5831–5838. (c) Kothandaraman, J.; Goepfert, A.; Czaun, M.; Olah, G. A.; Prakash, G. K. S. Conversion of CO₂ from Air into Methanol Using a Polyamine and a Homogeneous Ruthenium Catalyst. *J. Am. Chem. Soc.* **2016**, *138*, 778–781. (d) Treigerman, Z.; Sasson, Y. Generation and Quantification of Formate Ion Produced from Aqueous Sodium Bicarbonate in the Presence of Homogeneous Ruthenium Catalyst. *ACS Omega* **2018**, *3*, 12797–12801. (e) Zhang, L.; Han, Z.; Zhao, X.; Wang, Z.; Ding, K. Highly Efficient Ruthenium-Catalyzed N-Formylation of Amines with H₂ and CO₂. *Angew. Chem., Int. Ed.* **2015**, *54*, 6186–6189. (f) Kuhlmann, R.; Nowotny, M.; Künnemann, K. U.; Behr, A.; Vorholt, A. J. Identification of key mechanics in the ruthenium catalyzed synthesis of N,N-dimethylformamide from carbon dioxide in biphasic solvent systems. *J. Catal.* **2018**, *361*, 45–50. (g) Kar, S.; Sen, R.; Goepfert, A.; Prakash, G. K. S. Integrative CO₂ Capture and Hydrogenation to Methanol with Reusable Catalyst and Amine: Toward a Carbon Neutral Methanol Economy. *J. Am. Chem. Soc.* **2018**, *140*, 1580–1583. (h) Kar, S.; Sen, R.; Kothandaraman, J.; Goepfert, A.; Chowdhury, R.; Munoz, S. B.; Haiges, R.; Prakash, G. K. S. Mechanistic Insights into Ruthenium-Pincer-Catalyzed Amine-Assisted Homogeneous Hydrogenation of CO₂ to Methanol. *J. Am. Chem. Soc.* **2019**, *141*, 3160–3170. (i) Rezayee, N. M.; Huff, C. A.; Sanford, M. S. Tandem Amine and Ruthenium-Catalyzed Hydrogenation of CO₂ to Methanol. *J. Am. Chem. Soc.* **2015**, *137*, 1028–1031. (j) Liu, Q.; Wu, L.; Gülak, S.; Rockstroh, N.; Jackstell, R.; Beller, M. Towards a Sustainable Synthesis of Formate Salts: Combined Catalytic Methanol Dehydrogenation and Bicarbonate Hydrogenation. *Angew. Chem., Int. Ed.* **2014**, *53*, 7085–7088.

(10) (a) Monney, A.; Barsch, E.; Sponholz, P.; Junge, H.; Ludwig, R.; Beller, M. Base-free hydrogen generation from methanol using a bi-catalytic system. *Chem. Commun.* **2014**, *50*, 707–709. (b) Zhang, L.; Nguyen, D. H.; Raffa, G.; Trivelli, X.; Capet, F.; Desset, S.; Paul, S.; Dumeignil, F.; Gauvin, R. M. Catalytic Conversion of Alcohols into Carboxylic Acid Salts in Water: Scope, Recycling, and Mechanistic Insights. *ChemSusChem* **2016**, *9*, 1413–1423. (c) Kar, S.; Goepfert, A.; Prakash, G. K. S. Catalytic Homogeneous Hydrogenation of CO to Methanol via Formamide. *J. Am. Chem. Soc.* **2019**, *141*, 12518–12521. (d) Han, Q.; Xiong, X.; Li, S. An efficient, green and scale-up synthesis of amides from esters and amines catalyzed by Ru-MACHO catalyst under mild conditions. *Catal. Commun.* **2015**, *58*, 85–88. (e) Bornscheim, C.; Gustafson, K. P. J.; Verho, O.; Beller, M.; Bäckvall, J.-E. Evaluation of Fe and Ru Pincer-Type Complexes as Catalysts for the Racemization of Secondary Benzylic Alcohols. *Chem. - Eur. J.* **2016**, *22*, 11583–11586. (f) Thiyagarajan, S.; Gunanathan, C. Facile Ruthenium(II)-Catalyzed α -Alkylation of Arylmethyl Nitriles Using Alcohols Enabled by Metal-Ligand Cooperation. *ACS Catal.* **2017**, *7*, 5483–5490. (g) Oldenhuis, N. J.; Dong, V. M.; Guan, Z. From Racemic Alcohols to Enantiopure Amines: Ru-Catalyzed Diastereoselective

- Amination. *J. Am. Chem. Soc.* **2014**, *136*, 12548–12551. (h) Kishore, J.; Thiagarajan, S.; Gunanathan, C. Ruthenium(II)-catalysed direct synthesis of ketazines using secondary alcohols. *Chem. Commun.* **2019**, *55*, 4542–4545. (i) Li, Y.; Nielsen, M.; Li, B.; Dixneuf, P. H.; Junge, H.; Beller, M. Ruthenium-catalyzed hydrogen generation from glycerol and selective synthesis of lactic acid. *Green Chem.* **2015**, *17*, 193–198. (j) Alberico, E.; Lennox, A. J. J.; Vogt, L. K.; Jiao, H.; Baumann, W.; Drexler, H.-J.; Nielsen, M.; Spannenberg, A.; Checinski, M. P.; Junge, H.; Beller, M. Unravelling the Mechanism of Basic Aqueous Methanol Dehydrogenation Catalyzed by Ru-PNP Pincer Complexes. *J. Am. Chem. Soc.* **2016**, *138*, 14890–14904.
- (11) (a) Krishnakumar, V.; Chatterjee, B.; Gunanathan, C. Ruthenium-Catalyzed Urea Synthesis by N-H Activation of Amines. *Inorg. Chem.* **2017**, *56*, 7278–7284. (b) Thiagarajan, S.; Gunanathan, C. Ruthenium-Catalyzed α -Olefination of Nitriles Using Secondary Alcohols. *ACS Catal.* **2018**, *8*, 2473–2478. (c) Jankins, T. C.; Qin, Z.-Y.; Engle, K. M. A practical method for N-alkylation of phosphinic (thio)amides with alcohols via transfer hydrogenation. *Tetrahedron* **2019**, *75*, 3272–3281. (d) Thiagarajan, S.; Gunanathan, C. Catalytic Cross-Coupling of Secondary Alcohols. *J. Am. Chem. Soc.* **2019**, *141*, 3822–3827. (e) Thiagarajan, S.; Gunanathan, C. Ruthenium-Catalyzed Direct Cross-Coupling of Secondary Alcohols to β -Disubstituted Ketones. *Synlett* **2019**, *30*, 2027–2034.
- (12) (a) Chatterjee, B.; Gunanathan, C. Ruthenium Catalyzed Selective α - and α,β -Deuteration of Alcohols Using D₂O. *Org. Lett.* **2015**, *17*, 4794–4797. (b) Chatterjee, B.; Gunanathan, C. The ruthenium-catalysed selective synthesis of mono-deuterated terminal alkynes. *Chem. Commun.* **2016**, *52*, 4509–4512. (c) Zhang, L.; Nguyen, D. H.; Raffa, G.; Desset, S.; Paul, S.; Dumeignil, F.; Gauvin, R. M. Efficient deuterium labelling of alcohols in deuterated water catalyzed by ruthenium pincer complexes. *Catal. Commun.* **2016**, *84*, 67–70. (d) Krishnakumar, V.; Gunanathan, C. Ruthenium-catalyzed selective α -deuteration of aliphatic nitriles using D₂O. *Chem. Commun.* **2018**, *54*, 8705–8708.
- (13) A registered trademark of Takasago International Corporation. Kuriyama, W.; Matsumoto, T.; Ino, Y.; Ogata, O. PCT Int. Appl. Patent WO 2011048727A. 2011.
- (14) Bertoli, M.; Choualeb, A.; Lough, A. J.; Moore, B.; Spasyuk, D.; Gusev, D. G. Osmium and Ruthenium Catalysts for Dehydrogenation of Alcohols. *Organometallics* **2011**, *30*, 3479–3482.
- (15) Ding, K.; Han, Z. PCT Int. Appl. Patent WO 2014059757A1. 2014.
- (16) (a) Gunanathan, C.; Milstein, D. Metal-Ligand Cooperation by Aromatization-Deaeromatization: A New Paradigm in Bond Activation and “Green” Catalysis. *Acc. Chem. Res.* **2011**, *44*, 588–602. (b) Choi, J.-H.; Heim, L. E.; Ahrens, M.; Precht, M. H. G. Selective conversion of alcohols in water to carboxylic acids by in situ generated ruthenium trans dihydrido carbonyl PNP complexes. *Dalton Trans.* **2014**, *43*, 17248–17254. (c) Choi, J.-H.; Precht, M. H. G. Tuneable Hydrogenation of Nitriles into Imines or Amines with a Ruthenium Pincer Complex under Mild Conditions. *ChemCatChem* **2015**, *7*, 1023–1028. (d) Khusnutdinova, J. R.; Milstein, D. Metal-Ligand Cooperation. *Angew. Chem., Int. Ed.* **2015**, *54*, 12236–12273. (e) Bruch, Q. J.; Lindley, B. M.; Askevold, B.; Schneider, S.; Miller, A. J. M. A Ruthenium Hydrido Dinitrogen Core Conserved across Multielectron/Multi-proton Changes to the Pincer Ligand Backbone. *Inorg. Chem.* **2018**, *57*, 1964–1975.
- (17) The mass spectrum of **2** was reported: Krishnakumar, V.; Chatterjee, B.; Gunanathan, C. Ruthenium-Catalyzed Urea Synthesis by N-H Activation of Amines. *Inorg. Chem.* **2017**, *56*, 7278–7284.
- (18) Anaby, A.; Schelwies, M.; Schwaben, J.; Rominger, F.; Hashmi, A. S. K.; Schaub, T. Study of Precatalyst Degradation Leading to the Discovery of a New Ru⁰ Precatalyst for Hydrogenation and Dehydrogenation. *Organometallics* **2018**, *37*, 2193–2201.
- (19) He, T.; Buttner, J. C.; Reynolds, E. F.; Pham, J.; Malek, J. C.; Keith, J. M.; Chianese, A. R. Dehydroalkylative Activation of CNN- and PNN-Pincer Ruthenium Catalysts for Ester Hydrogenation. *J. Am. Chem. Soc.* **2019**, *141*, 17404–17413.
- (20) (a) Rodríguez-Lugo, R. E.; Trincado, M.; Vogt, M.; Tewes, F.; Santiso-Quinones, G.; Grützmacher, H. A homogeneous transition metal complex for clean hydrogen production from methanol-water mixtures. *Nat. Chem.* **2013**, *5*, 342–347. (b) Sinha, V.; Trincado, M.; Grützmacher, H.; de Bruin, B. DFT Provides Insight into the Additive-Free Conversion of Aqueous Methanol to Dihydrogen Catalyzed by [Ru(trop₂dad)]: Importance of the (Electronic) Flexibility of the Diazadiene Moiety. *J. Am. Chem. Soc.* **2018**, *140*, 13103–13114. (c) Govindarajan, N.; Sinha, V.; Trincado, M.; Grützmacher, H.; Meijer, E. J.; de Bruin, B. An In-Depth Mechanistic Study of Ru Catalysed Aqueous Methanol Dehydrogenation and Prospects for Future Catalyst Design. *ChemCatChem* **2020**, DOI: 10.1002/cctc.202000057 Recently, the same group has been able to extend their methodology to other substrates. (d) Casas, F.; Trincado, M.; Rodríguez-Lugo, R.; Baneerje, D.; Grützmacher, H. A Diaminopropane Diolenin Ru(0) Complex Catalyzes Hydrogenation and Dehydrogenation Reactions. *ChemCatChem* **2019**, *11*, 5241–5251.
- (21) Other related ruthenium-based systems that do not require a base as an additive have been reported: (a) Carrión, M. C.; Sepúlveda, F.; Jalón, F. A.; Manzano, B. R.; Rodríguez, A. M. Base-Free Transfer Hydrogenation of Ketones Using Arene Ruthenium(II) Complexes. *Organometallics* **2009**, *28*, 3822–3833. (b) García-Álvarez, R.; Suárez, F. J.; Díez, J.; Crochet, P.; Cadierno, V.; Antiñolo, A.; Fernández-Galán, R.; Carrillo-Hermosilla, F. Ruthenium(II) Arene Complexes with Asymmetrical Guanidinate Ligands: Synthesis, Characterization, and Application in the Base-Free Catalytic Isomerization of Allylic Alcohols. *Organometallics* **2012**, *31*, 8301–8311. (c) Muthaiah, S.; Hong, S. H. Acceptorless and Base-Free Dehydrogenation of Alcohols and Amines using Ruthenium-Hydride Complexes. *Adv. Synth. Catal.* **2012**, *354*, 3045–3053. (d) Canseco-Gonzalez, D.; Albrecht, M. Wingtip substituents tailor the catalytic activity of ruthenium triazolylidene complexes in base-free alcohol oxidation. *Dalton Trans.* **2013**, *42*, 7424–7432. (e) Dupau, P.; Bonomo, L.; Kermorvan, L. Unexpected Role of Anionic Ligands in the Ruthenium-Catalyzed Base-Free Selective Hydrogenation of Aldehydes. *Angew. Chem., Int. Ed.* **2013**, *52*, 11347–11350. (f) Kumar, M.; DePasquale, J.; White, N. J.; Zeller, M.; Papish, E. T. Ruthenium Complexes of Triazole-Based Scorpionate Ligands Transfer Hydrogen to Substrates under Base-Free Conditions. *Organometallics* **2013**, *32*, 2135–2144. (g) Tseng, K.-N. T.; Kampf, J. W.; Szymczak, N. K. Base-Free, Acceptorless, and Chemoselective Alcohol Dehydrogenation Catalyzed by an Amide-Derived NNN-Ruthenium(II) Hydride Complex. *Organometallics* **2013**, *32*, 2046–2049. (h) Delgado-Rebollo, M.; Canseco-Gonzalez, D.; Hollering, M.; Mueller-Bunz, H.; Albrecht, M. Synthesis and catalytic alcohol oxidation and ketone transfer hydrogenation activity of donor-functionalized mesoionic triazolylidene ruthenium(II) complexes. *Dalton Trans.* **2014**, *43*, 4462–4473. (i) Kim, K.; Kang, B.; Hong, S. H. N-Heterocyclic carbene-based well-defined ruthenium hydride complexes for direct amide synthesis from alcohols and amines under base-free conditions. *Tetrahedron* **2015**, *71*, 4565–4569. (j) Adam, R.; Alberico, E.; Baumann, W.; Drexler, H.-J.; Jackstell, R.; Junge, H.; Beller, M. NNP-Type Pincer Imidazolylphosphine Ruthenium Complexes: Efficient Base-Free Hydrogenation of Aromatic and Aliphatic Nitriles under Mild Conditions. *Chem. - Eur. J.* **2016**, *22*, 4991–5002. (k) Adam, R.; Bheeter, C. B.; Jackstell, R.; Beller, M. A Mild and Base-Free Protocol for the Ruthenium-Catalyzed Hydrogenation of Aliphatic and Aromatic Nitriles with Tridentate Phosphine Ligands. *ChemCatChem* **2016**, *8*, 1329–1334. (l) Cabrero-Antonino, J. R.; Alberico, E.; Drexler, H.-J.; Baumann, W.; Junge, K.; Junge, H.; Beller, M. Efficient Base-Free Hydrogenation of Amides to Alcohols and Amines Catalyzed by Well-Defined Pincer Imidazolyl-Ruthenium Complexes. *ACS Catal.* **2016**, *6*, 47–54. (m) Kim, D.; Kang, B.; Hong, S. H. Ruthenium-catalyzed selective imine synthesis from nitriles and secondary alcohols under hydrogen acceptor- and base-free conditions. *Org. Chem. Front.* **2016**, *3*, 475–479. (n) Sommer, M. G.; Marinova, S.; Krafft, M. J.; Urankar, D.; Schweinfurth, D.; Bubrin, M.; Košmrlj, J.; Sarkar, B. Ruthenium Azocarboxamide Half-Sandwich Complexes: Influence of the Coordination Mode on the Electronic Structure and Activity in Base-Free Transfer Hydrogenation Catalysis. *Organo-*

- metallics* **2016**, *35*, 2840–2849. (o) Kim, K.; Moeljadi, A. M. P.; Hirao, H.; Hong, S. H. Acceptorless and Base-free Dehydrogenation of Cyanohydrin with (η^6 -Arene)halide(Bidentate Phosphine)ruthenium(II) Complex. *Adv. Synth. Catal.* **2017**, *359*, 3292–3298. (p) Nguyen, D. H.; Raffa, G.; Morin, Y.; Desset, S.; Capet, F.; Nardello-Rataj, V.; Dumeignil, F.; Gauvin, R. M. Solvent- and base-free synthesis of wax esters from fatty acid methyl esters by consecutive one-pot, two-step catalysis. *Green Chem.* **2017**, *19*, 5665–5673. (q) Wang, Z.; Li, Y.; Liu, Q.-b.; Solan, G. A.; Ma, Y.; Sun, W.-H. Direct Hydrogenation of a Broad Range of Amides under Base-free Conditions using an Efficient and Selective Ruthenium(II) Pincer Catalyst. *ChemCatChem* **2017**, *9*, 4275–4281. (r) Farrar-Tobar, R. A.; Wei, Z.; Jiao, H.; Hinze, S.; de Vries, J. G. Selective Base-free Transfer Hydrogenation of α,β -Unsaturated Carbonyl Compounds using *i*PrOH or EtOH as Hydrogen Source. *Chem. - Eur. J.* **2018**, *24*, 2725–2734. (s) Le, L.; Liu, J.; He, T.; Malek, J. C.; Cervarich, T. N.; Buttner, J. C.; Pham, J.; Keith, J. M.; Chianese, A. R. Unexpected CNN-to-CC Ligand Rearrangement in Pincer-Ruthenium Precatalysts Leads to a Base-Free Catalyst for Ester Hydrogenation. *Organometallics* **2019**, *38*, 3311–3321. (t) Westhues, N.; Belleflamme, M.; Klankermayer, J. Base-Free Hydrogenation of Carbon Dioxide to methyl Formate with a Molecular Ruthenium-Phosphine Catalyst. *ChemCatChem* **2019**, *11*, 5269–5274.
- (22) (a) Pittaway, R.; Fuentes, J. A.; Clarke, M. L. Diastereoselective and Branched-Aldehyde-Selective Tandem Hydroformylation-Hemiaminal Formation: Synthesis of Functionalized Piperidines and Amino Alcohols. *Org. Lett.* **2017**, *19*, 2845–2848. (b) Wozniak, B.; Spannenberg, A.; Li, Y.; Hinze, S.; de Vries, J. G. Cyclopentanone Derivatives from 5-Hydroxymethylfurfural via 1-Hydroxyhexane-2,5-dione as Intermediate. *ChemSusChem* **2018**, *11*, 356–359.
- (23) For studies of BH_4^- by alcoholysis on related ruthenium complexes, see: (a) Belkova, N. V.; Bakhmutova-Albert, E. V.; Gutsul, E. I.; Bakhmutov, V. I.; Golub, I. E.; Filippov, O. A.; Epstein, L. M.; Peruzzini, M.; Rossin, A.; Zanobini, F.; Shubina, E. S. Dihydrogen Bonding in Complex $(\text{PP}_3)_2\text{RuH}(\eta^1\text{-BH}_4)$ Featuring Two Proton-Accepting Hydride Sites: Experimental and Theoretical Studies. *Inorg. Chem.* **2014**, *53*, 1080–1090. (b) Golub, I. E.; Filippov, O. A.; Belkova, N. V.; Gutsul, E. I.; Epstein, L. M.; Rossin, A.; Peruzzini, M.; Shubina, E. S. Competition between the Hydride Ligands of Two Types in Proton Transfer to $[\{\kappa^3\text{-P-CH}_3\text{C}(\text{CH}_2\text{CH}_2\text{PPh}_2)_3\}\text{RuH}(\eta^2\text{-BH}_4)]$. *Eur. J. Inorg. Chem.* **2017**, *2017*, 4673–4682.
- (24) Other groups have used phosphines to stabilize unsaturated ruthenium species: (a) Tseng, K.-N. T.; Kampf, J. W.; Szymczak, N. K. Base-Free, Acceptorless, and Chemoselective Alcohol Dehydrogenation Catalyzed by an Amide-Derived NNN-Ruthenium(II) Hydride Complex. *Organometallics* **2013**, *32*, 2046–2049. (b) Sun, Y.; Koehler, C.; Tan, R.; Annibale, V. T.; Song, D. Ester hydrogenation catalyzed by Ru-CNN pincer complexes. *Chem. Commun.* **2011**, *47*, 8349–8351. (c) Le, L.; Liu, J.; He, T.; Malek, J. C.; Cervarich, T. N.; Buttner, J. C.; Pham, J.; Keith, J. M.; Chianese, A. R. Unexpected CNN-to-CC Ligand Rearrangement in Pincer-Ruthenium Precatalysts Leads to a Base-Free Catalyst for Ester Hydrogenation. *Organometallics* **2019**, *38*, 3311–3321.
- (25) Ogata, O.; Nakayama, Y.; Nara, H.; Fujiwhara, M.; Kayaki, Y. Atmospheric Hydrogenation of Esters Catalyzed by PNP-Ruthenium Complexes with an N-Heterocyclic Carbene Ligand. *Org. Lett.* **2016**, *18*, 3894–3897.
- (26) Addison, A. W.; Rao, T. N.; Reedijk, J.; van Rijn, J.; Verschoor, G. C. Synthesis, structure, and spectroscopic properties of copper(II) compounds containing nitrogen-sulphur donor ligands; the crystal and molecular structure of aqua[1,7-bis(N-methylbenzimidazol-2'-yl)-2,6-dithiaheptane]copper(II) perchlorate. *J. Chem. Soc., Dalton Trans.* **1984**, 1349–1356.
- (27) Steiner, T. The Hydrogen Bond in the Solid State. *Angew. Chem., Int. Ed.* **2002**, *41*, 48–76.
- (28) (a) Dub, P. A.; Gordon, J. C. Metal-Ligand Bifunctional Catalysis: The “Accepted” Mechanism, the Issue of Concertedness, and the Function of the Ligand in Catalytic Cycles Involving Hydrogen Atoms. *ACS Catal.* **2017**, *7*, 6635–6655. (b) Gusev, D. G. Dehydrogenative Coupling of Ethanol and Ester Hydrogenation Catalyzed by Pincer-Type YNP Complexes. *ACS Catal.* **2016**, *6*, 6967–6981. (c) Nguyen, D. H.; Trivelli, X.; Capet, F.; Swesi, Y.; Favre-Réguillon, A.; Vanoye, L.; Dumeignil, F.; Gauvin, R. M. Deeper Mechanistic Insight into Ru Pincer-Mediated Acceptorless Dehydrogenative Coupling of Alcohols: Exchanges, Intermediates, and Deactivation Species. *ACS Catal.* **2018**, *8*, 4719–4734. (d) Shu, S.; Huang, M.; Jiang, J.; Qu, L.-B.; Liu, Y.; Ke, Z. Catalyzed or non-catalyzed: chemoselectivity of Ru-catalyzed acceptorless dehydrogenative coupling of alcohols and amines via metal-ligand bond cooperation and (de)aromatization. *Catal. Sci. Technol.* **2019**, *9*, 2305–2314.
- (29) Zell, T.; Langer, R. From Ruthenium to Iron and Manganese—A Mechanistic View on Challenges and Design Principles of Base-Metal Hydrogenation Catalysts. *ChemCatChem* **2018**, *10*, 1930–1940.
- (30) Examples of irreversible O–H addition to Ru^0 : (a) Huang, J.; Li, C.; Nolan, S. P.; Petersen, J. L. Solution Calorimetric Investigation of Oxidative Addition of HEAr (E = O, S, Se; Ar = $\text{C}_6\text{H}_4\text{X}$, X = CH_3 , H, Cl, NO_2) to $(\text{PMe}_3)_4\text{Ru}(\text{C}_2\text{H}_4)$: Relationship between HEAr Acidity and Enthalpy of Reaction. *Organometallics* **1998**, *17*, 3516–3521. (b) Kaplan, A. W.; Bergman, R. G. Nitrous Oxide Mediated Synthesis of Monomeric Hydroxoruthenium Complexes. Reactivity of $(\text{DMPE})_2\text{Ru}(\text{H})(\text{OH})$ and the Synthesis of a Silica-Bound Ruthenium Complex. *Organometallics* **1998**, *17*, 5072–5085. (c) Hirano, M.; Kurata, N.; Komiya, S. Successive O-H and sp^3 C-H bond activation of ortho-substituted phenols by a ruthenium(0) complex. *J. Organomet. Chem.* **2000**, *607*, 18–26.
- (31) Studies of oxidative addition to Ru^0 : (a) Hommeltoft, S. I.; Baird, M. C. Oxidative addition reactions of dicarbonyl[1,1,1-tris(diphenylphosphinomethyl)ethane]ruthenium(0). Elimination of ketene from an acetyl metal compound. *Organometallics* **1986**, *5*, 190–195. (b) Diggle, R. A.; Macgregor, S. A.; Whittlesey, M. K. Ability of N-Heterocyclic Carbene Ligands to Promote Intermolecular Oxidative Addition Reactions at Unsaturated Ruthenium Centers. *Organometallics* **2004**, *23*, 1857–1865. (c) Jaunky, P.; Schmalte, H. W.; Alfonso, M.; Fox, T.; Berke, H. Oxidative addition capability of triphosphine iron and ruthenium complexes with methyl iodide. *J. Organomet. Chem.* **2004**, *689*, 801–810. (d) Jaunky, P.; Schmalte, H. W.; Blacque, O.; Fox, T.; Berke, H. Iron(0) and ruthenium(0) complexes with tridentate phosphine ligands and their potential for ketene formation from methyl iodide, CO and a base. *J. Organomet. Chem.* **2005**, *690*, 1429–1455. (e) Cabeza, J. A.; Damonte, M.; García-Alvarez, P.; Pérez-Carreño, E. Reactivity of a (Bis-NHC)-tricarbonylruthenium(0) Complex with Methyl Triflate and Methyl Iodide. Formation of Methyl- and Acetylruthenium(II) Derivatives: Experimental Results and Mechanistic DFT Calculations. *Organometallics* **2013**, *32*, 4382–4390.
- (32) Chen, X.; Jing, Y.; Yang, X. Unexpected Direct Hydride Transfer Mechanism for the Hydrogenation of Ethyl Acetate to Ethanol Catalyzed by SNS Pincer Ruthenium Complexes. *Chem. - Eur. J.* **2016**, *22*, 1950–1957.
- (33) Dub, P. A.; Scott, B. L.; Gordon, J. C. Why Does Alkylation of the N-H Functionality within M/NH Bifunctional Noyori-Type Catalysts Lead to Turnover? *J. Am. Chem. Soc.* **2017**, *139*, 1245–1260.
- (34) (a) Jiang, Y.-Y.; Xu, Z.-Y.; Yu, H.-Z.; Fu, Y. A self-catalytic role of methanol in PNP-Ru pincer complex catalyzed dehydrogenation. *Sci. China: Chem.* **2016**, *59*, 724–729. (b) Kaithal, A.; Schmitz, M.; Hölscher, M.; Leitner, W. On the mechanism of the Ruthenium-catalyzed β -methylation of alcohols with methanol. *ChemCatChem* **2020**, *12*, 781.
- (35) (a) Lu, Y.; Liu, Z.; Guo, J.; Qu, S.; Zhao, R.; Wang, Z.-X. A DFT study unveils the secret of how H_2 is activated in the N-formylation of amines with CO_2 and H_2 catalyzed by Ru(II) pincer complexes in the absence of exogenous additives. *Chem. Commun.* **2017**, *53*, 12148–12151. (b) Puylaert, P.; van Heck, R.; Fan, Y.; Spannenberg, A.; Baumann, W.; Beller, M.; Medlock, J.; Bonrath, W.; Lefort, L.; Hinze, S.; de Vries, J. G. Selective Hydrogenation of α,β -Unsaturated Aldehydes and Ketones by Air-Stable Ruthenium NNS Complexes. *Chem. - Eur. J.* **2017**, *23*, 8473–8481. (c) Pinggen, D.; Choi, J.-H.; Allen, H.; Murray, G.; Ganji, P.; van Leeuwen, P. W. N. M.; Precht, M. H. G.;

Vogt, D. Amide versus amine ligand paradigm in the direct amination of alcohols with Ru-PNP complexes. *Catal. Sci. Technol.* **2018**, *8*, 3969–3976. (d) Agapova, A.; Alberico, E.; Kammer, A.; Junge, H.; Beller, M. Catalytic Dehydrogenation of Formic Acid with Ruthenium-PNP-Pincer Complexes: Comparing N-Methylated and NH-Ligands. *ChemCatChem* **2019**, *11*, 1910–1914.

(36) Durand, D. J.; Fey, N. Computational Ligand Descriptors for Catalyst Design. *Chem. Rev.* **2019**, *119*, 6561–6594.

(37) (a) Noyori, R.; Yamakawa, M.; Hashiguchi, S. Metal-Ligand Bifunctional Catalysis: A Nonclassical Mechanism for Asymmetric Hydrogen Transfer between Alcohols and Carbonyl Compounds. *J. Org. Chem.* **2001**, *66*, 7931–7944. (b) Noyori, R. Asymmetric Catalysis: Science and Opportunities (Nobel Lecture). *Angew. Chem., Int. Ed.* **2002**, *41*, 2008–2022.

(38) (a) Dub, P. A.; Henson, N. J.; Martin, R. L.; Gordon, J. C. Unravelling the Mechanism of the Asymmetric Hydrogenation of Acetophenone by [RuX₂(diphosphine)(1,2-diamine)] Catalysts. *J. Am. Chem. Soc.* **2014**, *136*, 3505–3521. (b) Dub, P. A.; Gordon, J. C. The mechanism of enantioselective ketone reduction with Noyori and Noyori-Ikariya bifunctional catalysts. *Dalton Trans.* **2016**, *45*, 6756–6781. (c) Dub, P. A.; Gordon, J. C. The role of the metal-bound N-H functionality in Noyori-type molecular catalysts. *Nat. Rev. Chem.* **2018**, *2*, 396–408.

(39) (a) Mandal, S. C.; Rawat, K. S.; Pathak, B. A computational study on ligand assisted vs. ligand participation mechanisms for CO₂ hydrogenation: importance of bifunctional ligand based catalysts. *Phys. Chem. Chem. Phys.* **2019**, *21*, 3932–3941. (b) Wei, Z.; de Aguirre, A.; Junge, K.; Beller, M.; Jiao, H. Exploring the mechanisms of aqueous methanol dehydrogenation catalyzed by defined PNP Mn and Re pincer complexes under base-free as well as strong base conditions. *Catal. Sci. Technol.* **2018**, *8*, 3649–3665. (c) Liu, C.; van Putten, R.; Kulyaev, P. O.; Filonenko, G. A.; Pidko, E. A. Computational insights into the catalytic role of the base promoters in ester hydrogenation with homogeneous non-pincer-based Mn-P, N catalyst. *J. Catal.* **2018**, *363*, 136–143.

(40) (a) Hasanayn, F.; Baroudi, A.; Bengali, A. A.; Goldman, A. S. Hydrogenation of Dimethyl Carbonate to Methanol by trans-[Ru(H)₂(PNN)(CO)] Catalysts: DFT Evidence for Ion-Pair-Mediated Metathesis Paths for C-OMe Bond Cleavage. *Organometallics* **2013**, *32*, 6969–6985. (b) Ye, X.; Plessow, P. N.; Brinks, M. K.; Schelwies, M.; Schaub, T.; Rominger, F.; Paciello, R.; Limbach, M.; Hofmann, P. Alcohol Amination with Ammonia Catalyzed by an Acridine-Based Ruthenium Pincer Complex: A Mechanistic Study. *J. Am. Chem. Soc.* **2014**, *136*, 5923–5929.

(41) Passera, A.; Mezzetti, A. Mn(I) and Fe(II)/PN(H)P Catalysts for the Hydrogenation of Ketones: A Comparison by Experiment and Calculation. *Adv. Synth. Catal.* **2019**, *361*, 4691–4706.

(42) While this work was under revision, a similar conclusion on Milstein's catalyst was published: Gusev, D. G. Revised Mechanisms of the Catalytic Alcohol Dehydrogenation and Ester Reduction with the Milstein PNN Complex of Ruthenium. *Organometallics* **2020**, *39*, 258–270.